PolyPublie
Polytechnique Montréal

POLYTECHNIQUE MONTRÉAL
UNIVERSITÉ D'INGÉNIERIE

Titre: Title:	Optical emission spectroscopic study of discharges
Auteur: Author:	You Bi
Date:	1993
Type:	Mémoire ou thèse / Dissertation or Thesis
Référence: Citation:	Bi, Y. (1993). Optical emission spectroscopic study of discharges [Mémoire de maîtrise, Polytechnique Montréal]. PolyPublie. https://publications.polymtl.ca/57020/

Document en libre accès dans PolyPublie
Open Access document in PolyPublie

URL de PolyPublie: PolyPublie URL:	https://publications.polymtl.ca/57020/
Directeurs de recherche: Advisors:	Michael R. Wertheimer, & Ludvik Martinu
Programme: Program:	Génie physique

Ce fichier a été téléchargé à partir de PolyPublie, le dépôt institutionnel de Polytechnique Montréal
This file has been downloaded from PolyPublie, the institutional repository of Polytechnique Montréal

https://publications.polymtl.ca

UNIVERSITE DE MONTREAL

OPTICAL EMISSION SPECTROSCOPIC STUDY OF DISCHARGES

PAR

You BI
DEPARTEMENT DE GENIE PHYSIQUE
ECOLE POLYTECHNIQUE

MEMOIRE PRESENTEE EN VUE DE L'OBTENTION
DU GRADE DE MAITRISE ES SCIENCES APPLIQUEES (M.Sc.A.)
(GENIE PHYSIQUE)

novembre 1993

©You Bi 1993

National Library of Canada

Acquisitions and Bibliographic Services Branch

395 Wellington Street
Ottawa, Ontario
K1A 0N4

Bibliothèque nationale du Canada

Direction des acquisitions et des services bibliographiques

395, rue Wellington
Ottawa (Ontario)
K1A 0N4

Your file Votre référence

Our file Notre référence

The author has granted an irrevocable non-exclusive licence allowing the National Library of Canada to reproduce, loan, distribute or sell copies of his/her thesis by any means and in any form or format, making this thesis available to interested persons.

L'auteur a accordé une licence irrévocable et non exclusive permettant à la Bibliothèque nationale du Canada de reproduire, prêter, distribuer ou vendre des copies de sa thèse de quelque manière et sous quelque forme que ce soit pour mettre des exemplaires de cette thèse à la disposition des personnes intéressées.

The author retains ownership of the copyright in his/her thesis. Neither the thesis nor substantial extracts from it may be printed or otherwise reproduced without his/her permission.

L'auteur conserve la propriété du droit d'auteur qui protège sa thèse. Ni la thèse ni des extraits substantiels de celle-ci ne doivent être imprimés ou autrement reproduits sans son autorisation.

ISBN 0-315-90039-3

Canadä

UNIVERSITÉ DE MONTRÉAL

ÉCOLE POLYTECHNIQUE

Ce mémoire intitulé:

OPTICAL EMISSION SPECTROSCOPIC STUDY OF DISCHARGES

présenté par: You BI

en vue de l'obtention du grade de: Maître ès sciences appliquées

a été dûment accepté par le jury d'examen constitué de :

M. NACHMAN, Manfred, D.Sc., président

M. WERTHEIMER, Michael R., D.Sc.A.,membre et directeur de recherche

M. MARTINU, Ludvik, Ph.D., membre et co-directeur de recherche

M. MOISAN, Michel, Ph.D., membre

Abstract

The objective of this work is to investigate the characteristics of discharges including reactive species concentration, ultraviolet (UV) and vacuum ultraviolet (VUV) radiation, and tail electron temperature under microwave (MW), radio frequency (RF), and dual-frequency (MW/RF) conditions.

Actinometry is employed to indicate the relative atomic oxygen concentration $[O]_r$ in O_2 plasma, and the relative atomic hydrogen concentration $[H]_r$ in Ar/CH_4 and N_2/CH_4 mixtures. In the $[O]_r$ study, the trends of $[O]_r$ are measured as a function of MW or RF power, axial position in the plasma reactor, oxygen pressure, and flow rate of O_2 feed gas. The $[O]_r$ values are found to be spatially non-uniform, and higher MW power or RF power and pressure result in larger $[O]_r$ values. The excitation channels of atomic oxygen emission lines at 777.1nm and at 844.6nm are also discussed. In the $[H]_r$ study, the trends of $[H]_r$ are investigated as a function of Ar and N_2 concentration in CH_4 feed. Increases of $[H]_r$ in CH_4 are found when Ar and N_2 are added.

A vacuum ultraviolet spectrometer is used to monitor the UV and VUV radiation from MW, RF, and MW/RF plasmas of Ar, O_2, CH_4, H_2, and N_2. Our results show that the MW/RF and the RF plasmas yield more intense radiation than that in the MW plasma.

The use of relative optical emission intensity ratio of different emission lines allows

us to monitor the temperature of tail electrons, with the assumptions of Maxwellian distribution and electron impact excitation. In this work, we present the experimental results of the dependence of tail electron temperature $T_e^{(t)}$ on axial position, MW power (or RF bias), and gas pressure in the argon plasma.

Sommaire

Au cours des dernières années, nous sommes témoins d'une augmentation rapide de l'importance des techniques plasma dans l'industrie de la microélectronique. Ils s'agit de techniques dites “sèches” qui tendent à remplacer les procédés chimiques en solutions liquides hazardeux et qui peuvent contaiminer les échantillons. Les méthodes par plasmas basses pressions se sont particulièrement distinguées par leur propreté, leur grande reproductibilité et leur adaptabilité pour l'automatisation. C'est grâce à ces caractéristiques que les techniques plasmas sont de plus en plus importantes dans d'autres domaines comme l'électrotechnologie, l'industrie de l'automobile, etc.

Habituellement, pour obtenir un plasma basse pression, on opère dans une intervalle de pression se situant entre 10^{-3} et 10 Torr. Ceci correspond à des densités électroniques de l'ordre de 10^9 à 10^{12} cm^{-3}, impliquant un faible niveau d'ionisation.

Le plasma basse pression peut être utilisé pour trois processus techniques importants, soient:

(i) l'enlèvement de matériau par gravure sèche;

(ii) le dépôt de films minces organiques (comme les polymères ou le diamant cristallin) et inorganiques (comme les matériaux isolants, semi-conducteurs et métalliques);

(iii) la modification de surface - dans ce cas, il n'y a ni d'enlèvement ni d'ajout de matériau, mais la composition et la structure des quelques couches de molécules à la surface de l'échantillon sont changées par le contrôle des paramètres de plasma pour soit améliorer l'adhésion, la mouillabilité, la tribologie, etc.

Les décharges radio-fréquentielles (RF: 13.56MHz) sont utilisées plus souvent pour les processus chimiques par plasma, comme la gravure du silicium. Pour ce qui est de

cette technique, le champ RF est couplé par capacité aux électrodes à l'intérieur du système de gravure. Les espèces actives provenant du plasma réagissent avec la partie exposée du substrat pour former des composés volatiles. Puisque l'enlèvement des produits de la gravure est l'étape qui limite le processus, on peut augmenter grandement l'efficacité en superposant un bombardement ionique - gravure ionique réactive ("reactive ion etching", RIE). Dans ce cas, les substrats sont placés sur l'électrode RF active où il y a une forte polarisation négative continue causée par la mobilité différente des électrons et des ions. Cependant, la technique RIE endommage la surface des échantillons à cause de ce bombardement ionique énergétique. Un autre problème se pose lorsque l'on considère l'incapacité d'opérer le plasma RF à de très basses pressions (< 1mTorr) pour réduire la contamination de surface et améliorer la qualité de la gravure. Une densité relativement faible du plasma constitue une autre limitation au plasma RF.

On porte une attention grandissante à l'utilisation du plasma excité par les fréquences micro-ondes (MW : 2.45GHz) pour le dépôt de films minces et pour la gravure de motifs. Généralement, le plasma MW offre des caractéristiques comme la création d'une haute densité d'ions de faibles énergies, une grande concentration d'espèces excités, et l'utilisation efficace du gaz. Pour ce mode de décharge, il n'y a pas d'électrodes directement exposées au plasma, ce qui a l'effet de réduire la possibilité de contamination provenant du procédé.

L'utilisation du plasma dans des domaines autres que la microélectronique requiert généralement des conditions qui permettent le traitement rapide de grandes surfaces. Il en est ainsi pour des applications comme les revêtements protecteurs en technologie spatiale, les barrières contre la perméation des gaz, les revêtements optiques, etc. A la lumière de ces nouveaux défis, il appert qu'une combinaision des avantages des modes de décharge RF et MW, sous le nom de plasma en mode double MW/RF, semble être une voie pleine de

promesse pour un meilleur contrôle de la gravure, et des dépôts. Pour la technique MW/RF, le substrat est placé sur l'électrode RF active tout en étant simultanément exposé au plasma MW, système qui permet le contrôle independant du flux et de l'énergie moyenne des ions qui bombardent le substrat.

Même si les traitements par plasma ont été utilisés depuis plusieurs décennies, les études qui examinent systématiquement l'effet de la fréquence sont relativement peu nombreuses; ceci s'applique particulièrement aux décharges MW/RF, où la très haute fréquence MW et la basse fréquence RF sont appliqués simultanément. De nouvelles connaissances sur ce type de décharge peuvent potentiellement conduire à une utilisation plus efficace des traitements par plasma.

Les plasma d'oxygène ont été utilisés abondamment pour le décapage de la photorésine, la gravure de polymères et l'application de multi-couches en VLSI (intégration à très grande échelle). Il existe certaines caractérisitiques nécessaires à une gravure efficace de la photorésine dont un taux de gravure élevé, un profil anisotrope, une grande sélectivité du substrat par rapport au masque, et de faibles dommages au substrat. La qualité de la gravure dépend des paramètres du plasma comme la puissance appliquée, la polarisation du substrat, la pression du gaz, le débit du gaz, etc. Puisque le taux de gravure en RIE dépend à la fois de l'énergie des ions et de la concentration des espèces, il est important de connaître la concentration d'oxygène atomique en function des paramètres du plasma pour une meilleure compréhension des processus chimiques et physiques dans le plasma.

Un autre procédé plasma de grand intérêt est d'obtenir, à basse pression, le dépôt de couches minces de diamant et de simili-diamant ("diamond like carbon", DLC) dans le méthane. La concentration d'hydrogène atomique est liée au niveau de décomposition du méthane. Une compréhension complète des mécanismes requiert, donc, l'étude de la

concentration de la concentration relative de l'hydrogène atomique $[H]_r$ dans le phase gazeuse du plasma.

En plus d'être une source d'espèces chimiquement réactives (par exemple, les atomes d'oxygène ou d'hydrogène), le plasma est ausi un émetteur de radiations électromagnétiques allant de l'ultraviolet lointain ("vacuum ultraviolet", VUV) jusqu'à l'infrarouge. Les photons UV et VUV sont capables d'initier des réactions photochimiques, par exemple le bris de liaisons covalentes C-H ou C-C au sein de matériaux polymériques.

Parmi les diverses méthodes utilisées comme diagnostic des processus physiques et chimiques dans le plasma, l'une des plus puissantes est la spectroscopie d'émission ("optical emission spectroscopy", OES). Elle permet d'identifier les espèces actives dans le plasma dont la désexcitation s'accompagne par une émission de photons, normalement dans la gamme de longueurs d'onde $200nm<\lambda<900nm$. L'appareillage requis pour cette fin comprend un monochromateur et un photodétecteur pour mesurer la lumière dispersée; l'appareil particulier utilisé dans nos études est un analyseur optique multicanaux ("optical multichannel analyser", OMA) dont le détecteur est une barette de 512 photodiodes.

La relation entre l'intensité d'émission optique provenant du plasma et la concentration de son espèce gazeuse à l'état fondamental est fort complexe, car la valeur de l'intensité mesurée dépend non seulement de la concentration de cette espèce mais aussi de la fonction de distribution en énergie des électrons ("electron energy distribution function", EEDF). Les deux, à leurs tours, dépendent des paramètres externes du plasma (pression, fréquence, puissance,...). La méthode dite "actinométrique" a été proposée pour la première fois en 1980 afin de pouvoir séparer l'effet de l'EEDF et celui de la concentration des espèces; selon cette méthode, le rapport d'intensités d'émissions optiques peut servir afin d'éstimer la concentration relative de certaines espèces à l'état fondamantal. En

particulier, l'intensité I_x provenant de l'espèce sous étude X, est comparée à la valuer I_A provenant du gaz actinométrique, un gaz ajouté au plasma en concentration faible et constante. Cette méthode de normalisation permet de compenser les variations de I_x dues aux variations du taux d'excitation liées, par exemple, à differentes EEDF, plutôt qu'à un changement en concentration de l'espèce à l'état fondamental. Les trois conditions nécessaires pour assurer que le rapport I_x/I_A est proportionnel à [X]/[A], le rapport des concentrations des espèces en jeu, sont les suivantes:

(i) les espèces excitées X et A sont produites à partir des atomes ou molécules à l'état fondamental par collisions électroniques;

(ii) le seul mode de désexcitation de X et A est par voie d'emission de photons;

(iii) les sections efficaces pour excitation par collisions électroniques de X et A sont caractérisées par des variations en fonction de l'énergie électronique et des seuils d'énergie très voisines.

L'objectif principal de cette recherche a été d'entreprendre une étude systématique des trois types de décharges(MW, RF et MW/RF) dans l'O_2 et le CH_4, à l'aide de la méthode actinométrique. Dans la premirère partie (section 3.1) l'actinométrie est comparée à d'autres méthodes diagnostiques des plasmas, tout en indiquant l'effet du choix d'un gaz actinométrique particulier. Les parties expérimentales principales (sections 3.2 et 3.3) sont consacrées à l'étude des effets de divers paramètres externes du plasma (puissance, pression, ...) sur le rapport I_x/I_A (X=O, H). On a également étudié sa variation spatiale entre les électrodes à l'aide d'un dispositif micrométrique conçu à cette fin, et l'on analyse ensuite les rendements relatifs des réactions en phase gazeuse pour les cas MW, RF et MW/RF. Ces résultats sont comparés à ceux provenant d'autres laboratoires, y compris des mesures absolues de [O] obtenues par voie de titration ou par spectrophotométrie VUV.

Pour le cas du plasma d'oxygène, l'actinométrie a été utiliseé pour mesurer la concentration relative d'oxygène atomique $[O]_r$, le gaz actinométrique principal utilisée étant l'argon (Ar); cependant, l'azote (N_2), lui-aussi, s'est avéré utile comme actinomètre. $[O]_r$ a été mesuré en fonction de la position axiale dans le réacteur, de la puissance MW (ou de la polarisation RF), de la pression, et du flux de gaz. La concentration relative $[O]_r$ s'est avérée être spatialement non-uniforme; une haute valeur de la puissance MW ou de la puissance RF et une pression élevée entraînent une valeur élevée de $[O]_r$. On a également étudié le mécanisme des excitations de l'oxygène atomique à 777.1 nm et à 844.6 nm. Dans le cas de l'hydrogène, la concentration relative $[H]_r$ dans le CH_4 a été étudiée en fonction du pourcentage d'Ar et de N_2. L'ajout de ces gaz a conduit à une augmentation de $[H]_r$ dans le CH_4.

Un spectrophotomètre ultraviolet a été utilisé pour étudier les rayonnements UV et VUV émis par des plasmas MW, RF et MW/RF d'Ar, O_2, CH_4, H_2 et N_2. Nos résultats montrent que les décharges MW/RF et RF émettent un rayonnement nettement plus intense que celui provenant du plasma MW.

L'utilisation du rapport relatif d'intensité d'émission optique provenant de différentes raies permet d'étudier la température d'électrons énergétiques sous l'hypothèse d'une distribution Maxwellienne et d'une excitation par collisions électroniques. Dans ce travail, nous présentons les résultats expérimentaux de la variation de la température électronique en fonction de la position axiale, de la puissance MW (ou de la polarisation RF) et de la pression partielle du gaz dans l'argon.

Acknowledgements

I would like to acknowledge gratefully my supervisor, Dr. Michel Wertheimer, for his intelligent guidance, his kindness, and his encouragements during my research work. My sincere thanks also to Dr. Ludvik Martinu, co-director, for his invaluable help, advice, and fruitful discussions, and for sharing his knowledge.

I wish to thank Mr. G. Jalbert for his technical assistance, and Dr. Edward Liston for his help and collaboration in vacuum ultraviolet spectroscopy.

I would also like to thank my parents for their encouragements in my academic work.

Table of Contents

PAGE

Abstract iv

Sommaire vi

Acknowledgements xii

Table of Contents xiii

List of Tables xvi

List of Figures xvii

List of Symbols xx

Chapter 1 Introduction 1

1.1 Low Pressure Plasma Processes 1

1.1.1 General Considerations 1

1.1.2 Plasma-Surface Interactions 4

1.2 Optical Emission Spectroscopy of Plasmas 6

1.2.1 General Considerations 8

1.2.1.1 Actinometry 9

1.2.1.2 Vacuum Ultraviolet Spectroscopy 13

1.2.2 Tail Electron Temperature 15

1.3 Objectives of This Work 16

Chapter 2 Experimental Methodology 18

2.1 Dual-Frequency Plasma Reactor 18

2.2 Optical Spectrometers 20

2.2.1 Optical Multichannel Analyser 20

2.2.2 VUV Spectrometer 21

Chapter 3 Experimental Results 22

3.1 The Effect of Actinometric Gases 22

3.1.1 Oxygen Plasma 22

3.1.2 Methane Plasma 24

3.2 Actinometry of Oxygen Discharge 27

3.2.1 The Effect of MW and RF Power 30

3.2.2 The Effect of Position in the Reactor 34

3.2.3 The Effect of Pressure 34

3.2.4 The Effect of Flow Rate 37

3.3 Actinometry of Methane Discharge 37

Chapter 4 Discussion 44

4.1 Oxygen Plasma 44

4.1.1 The Effect of Power Density 46

4.1.2 The Effect of Position in the Reactor 50

4.1.3 The Effect of Oxygen Pressure 51

4.1.4 The Validity of Actinometric Results 54

4.2 Methane Plasma 57

Chapter 5 Conclusion 60

References 62

Appendix 67

Appendix I Vacuum Ultraviolet Spectroscopy 68

Appendix II Measurement of the Tail Electron Temperature 77

II.1 Model 77

II.2 Results and Discussion 79

List of Tables

PAGE

Table 3.1 Species and transitions in O_2 discharge 32

Tabel 3.2 Species and transitions in CH_4 discharge 42

List of Figures

PAGE

Fig.1.1 Spectroscopic regions of the electromagnetic spectrum. 13

Fig.1.2 Schematic diagram of the resonance absorption apparatus. 14

Fig.2.1 Schematic illustration of the experimental apparatus. 19

Fig.3.1 Actinometric ratios of I_o at 844.6nm, I_{Ar} at 337.1nm, and I_{He} at 501.6nm as a function (a)MW power; (b)RF power; (c)MW power at a constant RF power 150W. Solid line (—): I_o/I_{Ar}; Dashed line (---): I_o/I_{N2}; and Dotted line (···): I_o/I_{He}. Pressure is 0.2Torr, O_2 flow rate is 55sccm, and total actinometers' flow rate is 2sccm. 23

Fig.3.2 Emission intensities of I_o at 777.1nm and at 844.6nm, and of I_{Ar} at 750.4nm as a function of the Ar percentage in the feed in the MW discharge. Total gas pressure is 0.2Torr, MW power is 200W. 25

Fig.3.3 Actinometric ratios of I_H at 656.3nm, and I_{Ar} at 750.4nm, I_{N2} at 501.6nm as a function of MW power in a CH_4 MW plasma at a pressure of 0.2Torr. Curve A: I_H/I_{Ar}; Curve B: I_H/I_{N2}; Curve C: I_H/I_{He}. 26

Fig.3.4 Emission intensity of I_H at 656.3nm as a function of Ar percentage in a 0.2Torr CH_4 plasma. MW power is 200W, total flow rate is 57sccm (4% N_2 as an actinometer). 28

Fig.3.5 Emission intensity of I_H at 656.3nm as a function of N_2 28

percentage in a 0.2Torr CH_4 plasma. MW power is 200W, total flow rate is 57sccm (4% Ar as an actinometer).

Fig.3.6 Actinometric ratio of I_o at 844.6nm and I_{Ar} at 750.4nm and emission intensity of I_o at 844.6nm line as a function of the MW power in an O_2 plasma. Pressure is 0.2Torr, and total flow rate is 57sccm (4% Ar as an actinometer). 29

Fig.3.7 Optical emission spectra from the O_2 discharge under MW, RF,and MW/RF conditions. The pressure is 0.2Torr, total flow rate is 57sccm (with 4% Ar as an actinometer). 31

Fig.3.8 The actinometric ratios R_1 (solid line —) and R_2 (dashed line ---) as a function of (a)MW power (b)RF power (c)MW power with a constant RF power 150W. The pressure is 0.2Torr, and total flow rate is 57sccm (4% Ar as an actinometer). 33

Fig.3.9 Optical emission spectra from the oxygen plasma under MW, RF, and MW/RF conditions at different locations between the MW applicator and the RF electrode. 35

Fig.3.10 Actinometric ratios R_1 (solid line —) and R_2 (dashed line ---) as a function of axial distance from the MW applicator in the O_2 plasma at 0.2Torr. Total flow rate is 57sccm (4% Ar as an actinometer). 36

Fig.3.11 Normalized actinometric ratios R_1/p_{Ar} (solid line —) and R_2/p_{Ar} (dashed line ---) as a function of O_2 pressure. The flow rate of O_2 and Ar are 55sccm and 2sccm, respectively. (a)MW power: 150W (b) RF power: 150W (c)MW/RF: 150W/150W. 38

Fig.3.12 Actinometric ratios R_1 (solid line —) and R_2 (dashed line ---) in the vicinity of the RF electrode as a function of O_2 flow rate. The pressure is 0.2Torr with 2sccm of Ar as an actinometer. (a)MW 39

power: 150W (b)RF power: 150W (c)MW/RF: 150W/150W.

Fig.3.13 Optical emission spectra for methane in the MW and the RF discharges. 41

Fig.3.14 Actinometric ratio I_H/I_{N2} as a function of the Ar percentage added to the CH_4 in the MW, RF, and MW/RF plasma (4% N_2 as an actinometer). 43

Fig.3.15 Actinometric ratio I_H/I_{Ar} as a function of the N_2 percentage added to the CH_4 in the MW, RF, and MW/RF plasma (4% Ar as an actinometer). 43

Fig.4.1 Actinometric ratio R_2 and dissociation degree Y as a function of power density. 47

Fig.4.2 Actinometric ratio R_2 and dissociation degree Y as a function of oxygen pressure. 52

Fig.4.3 Cross sections of electron impact excitation and dissociative excitation of I_o at 777.1nm and at 844.6nm. 56

List of Symbols

A	absorption rate
A_{ijx}	transition probability from i->j of species "X"
$[A]$	concentration of actinometer
$[Ar]$	concentration of argon
$[Br]$	concentration of bromine
$\mathbf{E}$	electric field
E_{th}	excitation threshold energy in general form
E_{thx}	excitation threshold energy of species "X"
E_{thA}	excitation threshold energy of species "A"
$[F]$	concentration of fluorine
$f(\varepsilon)$	electron energy distribution function
h	Planck's constant
$[H]$	concentration of atomic hydrogen
$[H]_r$	relative concentration of atomic hydrogen
I	emission intensity in general form
I_A	emission intensity of actinometer
I_{Ar}	emission intensity of argon
I_H	emission intensity of atomic hydrogen
I_{He}	emission intensity of helium
I_{N2}	emission intensity of molecular nitrogen
I_o	emission intensity of atomic oxygen
I_{ob}	intensity of atomic oxygen line at 130nm after traversing plasma

I_x	emission intensity of species "X"
K_v	volume excitation coefficient
m_e	mass of electron
N	neutral species density in ground state
n_e	electron density
[O]	concentration of atomic oxygen
$[O]_r$	relative concentration of atomic oxygen
p_A	partial pressure of actinometer
p_{Ar}	partial pressure of argon
P_{MW}	MW power
$P_{MW/RF}$	combination of MW and RF power
p_{O2}	partial pressure of oxygen
P_{RF}	RF power
R	actinometric ratio in general form
R_1	actinometric ratio of O at 777.1nm and Ar at 750.4nm
R_2	actinometric ratio of O at 844.6nm and Ar at 750.4nm
R_3	actinometric ratio of H at 656.3nm and N_2 at 337.1nm
R_4	actinometric ratio of H at 656.3nm and Ar at 750.4nm
T_e	electron temperature
$T_e^{(t)}$	tail electron temperature
v	electron velocity
[X]	concentration of species "X"
$[X]_r$	relative concentration of species "X"
Y	dissociation degree of molecular oxygen

$\sigma_A(\varepsilon)$	excitation cross section of actinometer
$\sigma_x(\varepsilon)$	excitation cross section of species "X"
ε	electron energy
$\Delta\varepsilon$	energy gap
θ	average power absorbed per electron from high frequency electric field
γ	wall recombination coefficient
λ	wavelength
ν_{ij}	excitation transition frequency from i->j in general
ν_{ijx}	excitation transition frequency from i->j of species "X"

CHAPTER 1

INTRODUCTION

1.1 Low Pressure Plasma Processes

Due to the prominence of plasma techniques in the semiconductor industry, there has been significant interest in low pressure plasma processing in recent years. The distinct advantages of low pressure plasma processing over conventional techniques include its capability for clean, highly reproducible and automatic operation. As a dry technique, plasma processing has begun to replace hazardous, polluting, wet-chemical processes in microelectronic fabrication.

This is also one of the reasons why plasma techniques are increasingly important for industrial applications in other fields such as electrotechnology, automotive industry, etc.

1.1.1 General Considerations

Plasma is the matter in the form of an electrified gas with the atoms and molecules partially dissociated into positive ions and negative electrons. In a plasma, the electrons are liberated from the atoms and acquire complete freedom of motion. With the loss of some of their electrons, atoms and molecules acquire a positive electric charge; they are then called

positive ions. Thus, a plasma is a gas consisting of positively and negatively charged particles in such proportions that the total charge is near zero. Freely moving charge carriers can transport electric current; in other words, a plasma is a conducting gas. The motion of particles in the plasma takes place in such a way that the ion cannot be separated from the electrons over distances exceeding the Debye length; this motion is termed collective. In general, plasma is defined as a quasineutral gas of charged and neutral particles which exhibits collective behavior. Usually low pressure plasma processes are performed in a range from 10^{-3} to about 10Torr. Typical electron densities are in the order of 10^{+9} - 10^{+12} cm^{-3} meaning a low degree of ionization (10^{-3} - 10^{-4}). In the plasma of electrical discharges, the electrons gain sufficient energy from the external electric field leading to ionization and excitation due to inelastic collisions with the gaseous species. Because of their high mobility and low collision frequency, the electrons in the plasma bulk possess a substantially higher energy (or temperature) than the other heavier species, and they initiate thermodynamically nonequilibrium physical and chemical processes.

Low pressure plasma can be used for three technologically important processes:

(i) etching - dry removal of materials.

(ii) deposition of organic (such as plasma polymers, or crystalline diamond) or inorganic thin films (such as insulating, semiconducting and metallic materials).

(iii) surface modification - in this process material is neither added nor removed, but the composition and structure of a few molecular layers at the materials' surface are controllably changed by the plasma, so as to improve adhesion, wettability, dye uptake, tribology, etc.

In the vicinity of a wall or for a surface immersed into the plasma, deviation from the quasineutrality occurs. In this region - the sheath - a potential drop exists which can accelerate the charged particles, because the surface is negative with respect to the plasma potential. Thus the positive ions contribute to the plasma-surface interactions. Ion

bombardment of the material surface can lead to sputtering, breakage of chemical bonds, ion incorporation, heating, and other forms of energy dissipation. These phenomena can be used to control the anisotropic plasma etching, growth, and microstructure of films (1-3).

The radio frequency (RF:13.56MHz) discharge has most often been employed for plasma chemical processes such as the etching of silicon. In this technique the RF field is capacitively coupled to the electrodes inside the etching system. The active species from the plasma react with the exposed substrate material forming volatile compounds. Since the removal of the etch products is the process-limiting step, this effect can be efficiently enhanced by superimposed ion bombardment - reactive ion etching (RIE). In RIE, the substrates are placed on the RF-powered electrode where a large negative direct current (DC) bias develops due to the difference in mobility of ions and electrons, and due to the possibility of a large ratio of the grounded and powered electrode areas. However, the RIE technique is known to cause damage at the sample surface because of this energetic ion bombardment. Another problem arises due to an incapability to operate the RF plasma at low pressures (<1mTorr) which would reduce surface contamination and improve etching patterns. A relatively low plasma density is another limitation of RF plasma.

Increasing attention is being paid to the use of plasma excited at microwave (MW) frequencies (e.g. 2.45GHz) for thin film deposition or pattern etching (4). Generally, the MW plasma offers other features, such as the generation of a high density of low energy ions, a high concentration of excited species, and efficient gas utilization (5). In the MW discharge there are no electrodes directly exposed to the plasma (which can contaminate the process). Also, MW plasma can be operated at low pressure.

On the other hand, the use of plasma in the reactors other than microelectronics requires the conditions which allow processing of large areas at high rates and at low substrate temperature. This applies for materials such as protective coating for space technology, barriers against gas permeation, optical coatings etc (4). In the light of the new

challenges, a combination of the advantages of both the RF and the MW discharges in the so called dual mode MW/RF plasma appears very promising (6) for better control of etching or deposition. In this MW/RF technique the substrate is placed on the RF powered electrode while being simultaneously exposed to the MW plasma. This arrangement allows us to control the electron density and the energy of ion flux independently (7, 8).

Even if plasma processes have been used for several decades, the number of works systematically investigating the effect of frequency is relatively limited (9, 10). This applies particularly to the MW/RF discharge, where a high frequency (MW) and a lower frequency (RF) power are applied simultaneously. The further development in this subject is needed. The new knowledge of MW/RF plasma will lead to the better using of plasma technique.

1.1.2 Plasma-Surface Interactions

Plasma represents a very complex environment, and associated plasma-surface interactions can affect an exposed material's microstructure and properties. The plasma-surface interactions include ion bombardment, the effect of reactive species on the surface, and the effect of irradiation by energetic photons.

Oxygen plasmas have been used extensively for photoresist stripping, polymer etching, and multilayer resist application in VLSI (very large scale integration) (11-13). Some requirements for photoresist etching may include high etch rate, anisotropic profile, high selectivity over the substrate and mask, and low substrate damage. The etching quality has been found (14,15) to depend on plasma parameters including applied power, substrate bias, gas pressure, and flow rate etc. Since the etch rate in RIE depends on both ion energy and species concentration, the knowledgement of atomic oxygen concentration as a

function of plasma parameters is required for better understanding of chemical and physical processes in the plasma.

Atomic oxygen interaction with polymers is also important because polymers are widely used as spacecraft materials. The operation of many spacecraft has shown that atomic oxygen seriously erodes polymers used as a functional materials (16). In low earth orbit (LEO) the concentration of molecular oxygen in space environment appears to be insignificant compared to that at the earth's surface (17), but the actual flux of atoms impinging on an orbiting vehicle is quite high because of the satellite orbital velocity of 8km/sec, which corresponds to an incident atomic oxygen energy of 5eV. The investigation of oxygen atom concentration [O] in ground-based systems for simulation of the neutral atomic oxygen environment in LEO is useful in studying of the effects of atomic oxygen on the erosion of polymer based materials.

The plasma processing used for diamond and diamond like carbon (DLC) film deposition at low pressure is also of great interest, and it is currently being investigated in this laboratory (2,7,18,19). In 1981, Spitsyn et al. (20) suggested that atomic hydrogen is the species responsible for the etching of graphite during the diamond growth process. Since that time, the role of atomic hydrogen is regarded as being very important for diamond growth, in which the methane based plasma is widely used for diamond and DLC deposition. The methyl radical CH_3 is considered as the principal species responsible for diamond or DLC film growth (21-23); hence, the atomic hydrogen concentration is coupled to the degree of decomposition of methane. The experimental results of this laboratory mentioned above confirm that atomic hydrogen in DLC deposition is an important factor. A complete understanding of the mechanism requires investigation of atomic hydrogen concentration [H] in the gas phase in methane based plasma.

Besides the optical emission spectrum in visible and near infrared regions, the ultraviolet (UV) and vacuum ultraviolet (VUV) emission from low pressure plasma is also

important in plasma processing, as the radiation from plasma may cause damage on the substrate. Usually the plasma damage is referred to the undesirable changes that occur to materials exposed to plasmas. The manifestation of damage depends on the discharge properties, on the species present in the plasma, and on the properties of the material that is exposed to the plasma. Recent studies (24,25) show that the plasma induced damage is not only a result of high ion energies but also of long plasma exposure times, probably due to the greater accumulation of UV and VUV radiation effects.

In treatment of polymers, the radiation can cause crosslinking on the surface of the polymer. Crosslinking occurs in polymer surfaces exposed to plasmas which are effective at creating free radicals in the polymer: the VUV and UV light attacks the polymer surface and breaks C-C and C-H bonds, leaving radicals in the surface. For example, almost all of the observed radiation from an oxygen plasma is from the first excited state of the oxygen radical at 1302Å (26). A photon at this wavelength has an energy of 220Kcal/mole, which is about double the bond strength of the C-C or C-H bond, so that the radiation can readily cause vacuum-ultraviolet photochemistry.

The plasma generally acts as a broad-band UV lamp, for it can contain spectral emissions in the range from a few tens to a few hundreds of nanometers. Since the UV absorbed energy obeys Beer's law (27), the UV radiation intensity is an important parameter which affects materials surfaces.

1.2 Optical Emission Spectroscopy of Plasmas

Various plasma diagnostics are used for the study of plasma parameters and of the physical and chemical processes. The principal diagnostic tools that are currently employed for basic investigation and for technological applications include the following: Langmuir

probes, mass (or ion) spectroscopy, optical emission spectroscopy (OES), microwave interferometry, laser techniques (eg. laser induced fluorescence), and others. The diagnostic measurements provide plasma parameters such as electron temperature T_e, electron density n_e, gas composition, concentrations of ground state or excited species, neutral or ionized, electric field distribution, electron energy distribution function (EEDF), etc.

Diagnostic techniques can be divided into two general categories: ex situ, and in situ. The common characteristic of ex situ techniques is that they sample a specific amount of the plasma reactor's contents, and transfer it elsewhere for examination. These analytical techniques include neutral and ion mass spectroscopy, chemical titration via downstream reaction, etc. An advantage of the ex situ techniques is that they allow the full power of numerous analytical techniques to be employed. The main drawback of ex situ techniques is that the concentrations of many highly reactive species, ions, free radicals, can be largely modified during their journey from the reactor.

The in situ techniques can be divided into two groups: intrusive and non-intrusive. An example of an in situ intrusive technique is the use of a Langmuir probe, which is directly immersed into the plasma. On the other hand, the OES technique can be used in-situ, but it does not perturb the plasma.

One of the very powerful techniques is laser diagnostics. During the past twenty-five years these techniques were developed rapidly, which allow characterization of complex discharges; they can be used for the measurement of electron and ion densities, the vibrational and rotational temperatures, or levels of particle populations. This technique is also suitable for the measurement of the ground state concentration of species (28), and measurements of the local electric field (29,30). In general, however, it is still difficult to measure energy distributions by this approach.

1.2.1 General Considerations

The completely non-intrusive technique of OES consists of the analysis of optical emission from the plasma zone. The emission characteristics are related to the concentrations of active species such as atoms, radicals, excited molecules, and which results in photons emitted in the vacuum ultraviolet (VUV), near UV, and the visible regions.

Plasma-induced emission can arise from electron impact excitation,

$$X + e \rightarrow X^* + e \qquad (1)$$

electron impact dissociation

$$XY + e \rightarrow X^* + Y + e \qquad (2)$$

or an ion impact process,

$$X^+ + e(+M) \rightarrow X^*(+M) \qquad (3)$$

where X and Y are atoms or molecules, * indicates the excited emitting species, and e(+M) may be a neutral species, a negative ion, an electron plus a third body, or a surface.

If emission mainly arises from reaction (1), then the emission intensity of species X is given by (31):

$$I_x \propto X^* \propto n_e[X] \int_{E_{thx}}^{\infty} f(\varepsilon)\sigma_x \sqrt{\frac{2\varepsilon}{m_e}}\, d\varepsilon \qquad (4)$$

where [X] is the ground state concentration of species "X", ε is the electron energy, $\sigma_x(\varepsilon)$ is the electron impact excitation cross section, $f(\varepsilon)$ is the electron energy distribution function (EEDF), E_{thx} is the threshold energy for the process under consideration.

The equation (4) indicates that (i) the OES technique relies on the detection of emission from plasma species in excited electronic states (associated with [X]*); (ii) the emission intensity depends on the electron density n_e, species concentration [X], excitation

cross section $\sigma_x(\varepsilon)$, and the EEDF. (iii) OES is suitable to identify species in plasma, due to $\sigma_x(\varepsilon)$ and E_{thx} being species-specific.

Usually, OES techniques can be used to identify the species emitting from plasma in the spectral region between 200nm and 900nm. This is because the OES requires a monochromator to disperse the plasma emission and a photodetector to measure the dispersed radiation. In the region mentioned above, silicon detectors (used most often) have adequate sensitivity. In the VUV region (below 190nm), vacuum enclosures are required to prevent absorption by air or by window materials.

In general, the spectrum from electronic transitions (difference of energy levels $\Delta\varepsilon$ = 1-20eV) occurs in near infrared, visible, and UV regions. The spectrum from rotationally excited levels ($\Delta\varepsilon < 0.5$eV) and vibrationally excited levels ($\Delta\varepsilon = 0.05 - 1.0$eV) occurs in the infrared (IR) region. Since these signals ($\lambda > 190$nm) are many orders of magnitude weaker than visible-UV radiation, these emissions must be monitored by an IR-detector. Consequently, relatively few studies have been performed in the IR region for low pressure plasma.

1.2.1.1 Actinometry

The relationship between the optical emission intensity and the species concentration of feed gas in the ground state is quite complicated. From equation (4), we notice that it is not straightforward to derive the value of [X] from I_x directly, since the value of intensity depends not only on the concentration but also on the EEDF, and both the species concentration in the ground state and the EEDF depend on the technique conditions..

In the actinometric technique, proposed in 1980 (32) to separate the effects of species concentration and EEDF, the ratio of optical emission intensity provides an estimate

of relative species concentrations in the ground state. The value of I_x from the species of interest is compared to that of I_A from an actinometer - a gas added to the plasma in small, constant quantities. This normalization compensates the changes in I_x values due to the variations of excitation rate, resulting, for example, from a different EEDF, rather than from an actual change in the species concentration in the ground state. The following three conditions are necessary to ensure that the emission intensity ratio I_X/I_A is proportional to the concentration ratio [X]/[A], of the species of interest X and of the actinometer A:

(i) the excited species X and A are produced by electron impact excitation of the ground state atoms or molecules;

(ii) the excited species decay only by photon emission;

(iii) the electron impact excitation cross sections for X and A have similar excitation threshold energies and shapes as a function of electron energy.

Conditions (i) and (iii) are used to ensure a similar behavior of the species of interest and of the actinometer in the discharge. Condition (ii) is important for the use of OES as a diagnostic technique.

When the conditions mentioned above are satisfied, electron impact excitation is balanced by optical emission, and the proportionality constant C in the relationship below is demonstrated to be independent of plasma parameters (31, 32):

$$\frac{I_x}{I_A} \propto \frac{[X]}{[A]} \frac{\int_{E_{thx}}^{\infty} f(\varepsilon)\, \sigma_x(\varepsilon) \sqrt{\frac{2\varepsilon}{m_e}}\, d\varepsilon}{\int_{E_{thA}}^{\infty} f(\varepsilon)\, \sigma_A(\varepsilon) \sqrt{\frac{2\varepsilon}{m_e}}\, d\varepsilon} = C\frac{[X]}{[A]} \quad (5)$$

where σ_x and σ_A are excitation cross sections, ε is the electron energy, E_{thx} and E_{thA} are the excitation threshold energies, and C is a constant. We can write the equation (5) in the shorter form

$$[X] \propto [I_x/I_A][A] \quad (6)$$

here the term I_X/I_A is called the actinometric ratio in actinometry technique (31,32); [A] is the concentration of actinometer, and [X] is defined in equation (4).

From the above relation we can see that the species concentration [X] is proportional to the product of the actinometric ratio I_X/I_A and actinometer concentration [A]. So that, [X] varies directly with the change of I_X/I_A at a constant [A]. When Coburn and Chen (32) developed the actinometry model, they use this relation to monitor [X]. Usually, [A] must be constant in this technique.

Here, however, the equation (6) just provides the proportionality relation between I_X/I_A and [X]; it does not give us the numerical value of [X], in other words, the actinometry technique cannot be used as an absolute measure of species concentration. The actinometric ratio I_X/I_A being in arbitrary units, it just tells us the relative value of [X]. In the following work, the respective actinometric ratios in arbitrary units are employed as a estimation of relative atomic oxygen concentration $[O]_r$ and relative atomic hydrogen concentration $[H]_r$ as function of various discharge conditions.

Notice that a constant [A] is required in the actinometry model. Indeed, the direct proportion relation between I_X/I_A and [X] holds only when [A] = constant is satisfied(see equation 6). To extend this model to the study of pressure dependence, where the percentage of actinometer in the feed gas is constant but [A] rises with the total pressure, Coburn and Chen (33) used the normalized actinometric ratio (which is obtained by dividing the actinometric ratio I_X/I_A by the actinometer's partial pressure p_A so as to obtain I_X/I_A at constant actinometer concentration) as a measure of [X]. In other words, the normalized actinometric ratio $(I_X/I_A)/p_A$ then replaces the actinometric ratio I_X/I_A to represent the relative value of [X] in a pressure dependence study.

From the above description of the actinometry model, we have found that the actinometric ratio may serve as a measure of the relative concentration of species. So far this model has been very successful in a variety of plasmas: Donnelly and co-workers (34)

have monitored F atoms downstream from the discharge, compared with an evaluation using chemical titration. The authors found that the I_F/I_{Ar} ratio well reflects [F] in $CF_4/O_2/Ar$ and in NF_3/Ar plasmas. Ibbotson et al (35) used Ar as an actinometer for [Br] monitoring in Br_2 plasma. In their work, the Br_2 concentration was measured by absorption spectroscopy, and [Br] was deduced from reduction of Br_2 concentration due to dissociation in the plasma. The I_{Br}/I_{Ar} ratio was found to follow the [Br] value. Actinometry has been applied for CCl_4 discharges by Tiller et al. (36). A quantitatively reliable measurement of CCl concentration has been confirmed by laser-induced fluorescence (LIF) spectroscopy. Of particular importance has been the use of actinometry in oxygen-containing discharges: the relative concentration of atomic oxygen $[O]_r$ in the O_2 and the O_2/CF_4 plasmas has been measured by Walkup et al (37), and compared with the data from LIF measurement. In their actinometric approach the authors used the lines I_o-844.6nm and I_{Ar}-750.4nm. The ratio I_o/I_{Ar} was found to follow the independently determined [O] value over a wide range of conditions, including the variations of RF power and percentage of CF_4. Recently, the observations mentioned above has been confirmed by Amorim et al (38) for the case of a discharge in pure oxygen.

Mucha et al. (39) measured the relative atomic hydrogen concentration $[H]_r$ in a diamond growth system ($CH_4/H_2/O_2$) using actinometry, where values of $[H]_r$ are monitored using the relative intensity of the hydrogen Balmer line (656.3nm) to the Ar line (750.4nm). The Balmer line (656.3nm) was also used by other groups to monitor $[H]_r$ in plasma of hydrogen-containing gases including CH_4, CH_4/H_2, and $CO/H_2/He$, all in plasma deposition of DLC (40-42).

We have now seen that the actinometry technique appears to be successful in the measuring of various species relative concentration in different plasmas.

1.2.1.2 Vacuum Ultraviolet (VUV) Spectroscopy

Low pressure plasma is a source of electromagnetic radiation extending from VUV

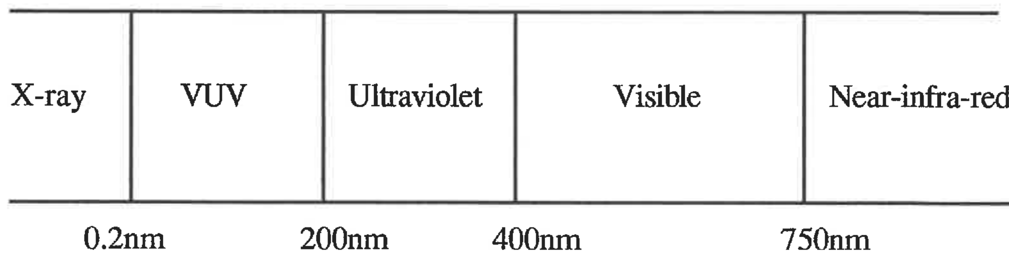

Fig.1.1 Spectroscopic regions of the electromagnetic spectrum.

to the infra-red (IR) regions (see Figure 1.1). We can see that the entire vacuum ultraviolet region is down to about 0.2nm. Thus the VUV region overlaps the soft X-ray region (0.2-30nm). The difference between the regions is simply that VUV or optical radiation corresponds to energy changes of the outer electrons of an atom or ion, while X-radiation corresponds to energy changes of the inner electrons.

Until now, most studies of the plasma-materials interactions have been oriented towards the effects of ions, electrons, and neutral species, while only very few studies have been devoted to effects involving UV photons, particularly VUV radiation. Difficulties in this latter region mainly arise from the absorption of radiation by matter below 190nm, and from a lack of materials transparent at $\lambda \leq 110$nm. For high pressure, high temperature plasma, the spectral lines and the continuum radiation are far stronger in the VUV region than in the visible and near UV, while VUV radiation from low pressure plasma is relatively weak. VUV spectra from low pressure cold plasma have been reported

(26, 43), the main modification in experimental procedure resides in evacuation of the spectroscopic system.

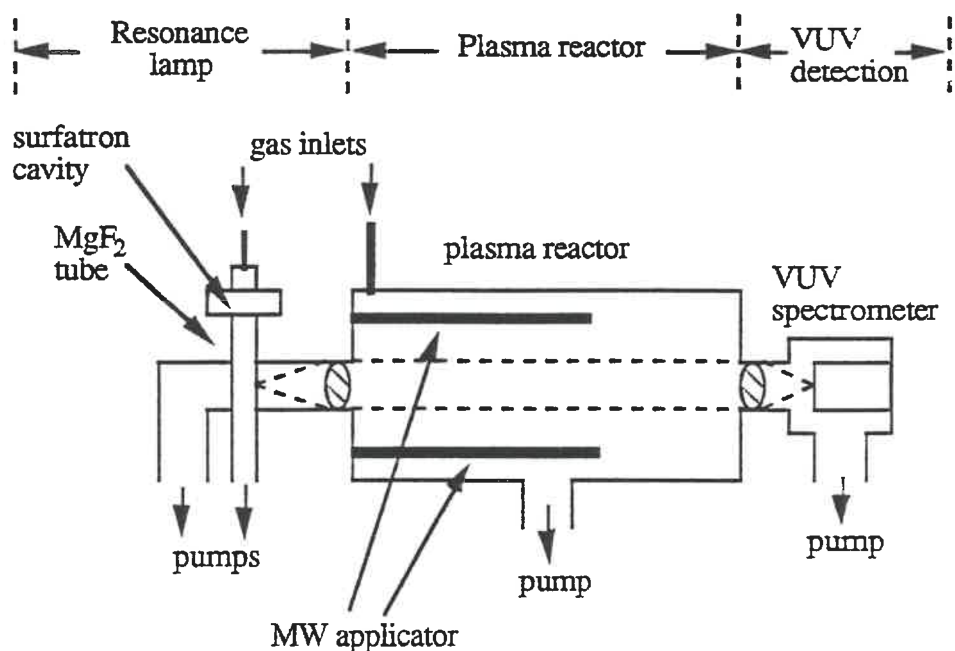

Fig.1.2 Schematic diagram of the resonance absorption apparatus(from Ref.45).

Recently, absolute oxygen atom concentrations in plasmas have been determined by VUV resonance absorption at 130nm (38,44,45). In this method an independently excited source is used to produce resonance radiation at 130nm from atomic oxygen. This light is passed through the plasma where it is attenuated due to absorption by ground state oxygen atoms (see figure 1.2). The attenuation of the beam intensity may be directly related to the number of atoms in the optical path with a knowledge of the transition probability and of the spectral profiles of the source emission and of the absorption. The observed absorption rate is given by

$$A = 1 - (I_{oa} / I_{ob}) \qquad (7)$$

Here I_{ob} is the initial source intensity (before passing through the plasma) and I_{oa} is the intensity after passing plasma.

The dependence of A on the ground state atomic oxygen concentration can be calculated by integrating numerical method. The details of calculation of the dependence of the absorption rate on the O atom concentration are given by Refs.44 and 45. Comparing the observed A and the calculated one, the absolute atomic oxygen concentration can be obtained.

In order to measure [O] using this method, it is necessary to have an independent excitation source to produce the O emission line at 130nm. In our laboratory, we do not have this capability. Therefore, we cannot perform this measurement. An alternative approach for determining [O] is titration with NO_2 (50).

1.2.2 Tail Electron Temperature

It is known that the majority of the electrons involved in the plasma collision processes, such as excitation and ionization, are those with sufficiently high energy. These electrons absorb energy from the external by applied field, and produce the reactive neutrals and ions. Therefore, understanding the electron kinetic energy, i.e. the electron temperature, is important to an understanding of plasma processes.

To study the energetic electrons in low pressure plasma, a two-electron group model (2-EGM) was proposed by Vriens in 1973 (46). According to this model, electrons in the plasma can be distinguished into two groups: one group represents the bulk electrons with electron energies $\varepsilon < E_{th}$, while the second group represents the "tail electrons" with energies $\varepsilon > E_{th}$ (E_{th} being the first inelastic threshold energy). In this way, the 2-EGM

specifies the high-energy tail of the electron energy distribution with an electron temperature different from that of the bulk: the tail temperature. The most important feature of 2-EGM, then, is the subdivision of the electrons into two different groups, each described by it's own characteristic temperature.

Since the tail electron group has a high energy, it is very effective in interacting with neutral species in the plasma. In previous studies, the high-temperature electron tail phenomena have been studied using Langmuir probes. Rossnagel and Kaufman (47) reported the presence of a high-temperature electron tail in a He discharge. Sheridan et al. (48) investigated the tail temperature in a sputtering magnetron plasma. However, few optical spectroscopic measurements of tail electron temperature of plasmas have so far been reported. Since optical emission is excited by electrons with energies above the excitation threshold, it is the tail electrons which are mainly responsible for optical emission from low pressure plasma, i.e. tail electron group of 2-EGM. Thus, the optical emission from the plasma should be related to the tail electron group. In this work we develop a method to estimate the tail electron temperature $T_e^{(t)}$ using optical emission spectroscopy.

1.3 Objectives of This Work

The principal aim of the present work is to systematically study the characteristics of three types of discharges, namely MW, RF and MW/RF. This investigation will be done for two different considerations leading to (i) plasma etching, such as in an oxygen plasma, and (ii) plasma deposition, such as in a case when methane is used. The effects will be studied using optical emission spectroscopy (OES), and its modification known as actinometry.

In the first part of this work (section 3.1) the actinometric approach mentioned above will be described and compared to other plasma diagnostic methods. Then, the effect of different actinometric gases on the diagnostic measurements will be studied. The principal part of the experimental study (section 3.2 and 3.3) will be devoted to the effects of various external plasma parameters (such as power, pressure, etc) on the actinometric ratio, which indicates the relative species concentrations in the plasma of oxygen (atomic oxygen O) and methane (atomic hydrogen H). The spatial distributions of actinometric ratio in the interelectrode region is also investigated. The results will then be analyzed with respect to the efficiency of gas phase reactions in MW, RF and MW/RF plasma, and will be compared with the results of other workers, for example, with the results from VUV measurements.

In the Appendix I, radiation emitted from the plasma in the UV and VUV region (down to wavelength 110nm) will be analysed, and the characteristics of the MW, RF, and MW/RF discharges will be compared.

In the Appendix II, we describe a method to evaluate the average temperature of tail electron group $T_e^{(t)}$ by using OES in an Ar plasma under the MW, RF, and MW/RF conditions. We present the experimental results of dependence of $T_e^{(t)}$ on plasma parameters such as power, pressure, and axial position.

CHAPTER 2

EXPERIMENTAL METHODOLOGY

2.1 Dual-Frequency Plasma Reactor

The experimental set-up is shown schematically in Fig.2.1. The microwave (2.45GHz) power from a 1.5kW generator is delivered to the vacuum chamber by a rectangular periodic slow-wave structure. The incident, reflected and transmitted powers are monitored via directional couplers, and indicated on power meters. A three stub tuner is used for adjustment of minimum reflected power. The slow-wave structure delivers the MW electromagnetic field energy into the plasma chamber through a fused silica window, and it thereby excites the MW discharge, while the power transmitted through the slow-wave structure is absorbed by a high power dry load.

The plasma chamber is a 510x150x615mm rectangular steel vessel. The RF (13.56MHz) aluminum cathode (150mm in diameter), is placed at a distance of 32mm from the window, and it is capacitively coupled to the RF power supply. The forward and reflected RF powers are monitored using RF power meters, and the RF-induced negative dc self-bias voltage on the cathode is measured with respect to ground, using an RF choke.

The plasma is produced in the space between the window and the RF cathode in a region of about 300x32x150mm. In this so-called "large volume microwave plasma (LMP)" system, the plasma can be generated either with "pure" RF or MW excitation, or in a dual-frequency MW/RF mode, when both power sources are activated simultaneously.

A turbomolecular pump, backed by a rotary pump, is used to provide the base pressure of 10^{-4}Torr. During experiment, the working gas mixture was adjusted using

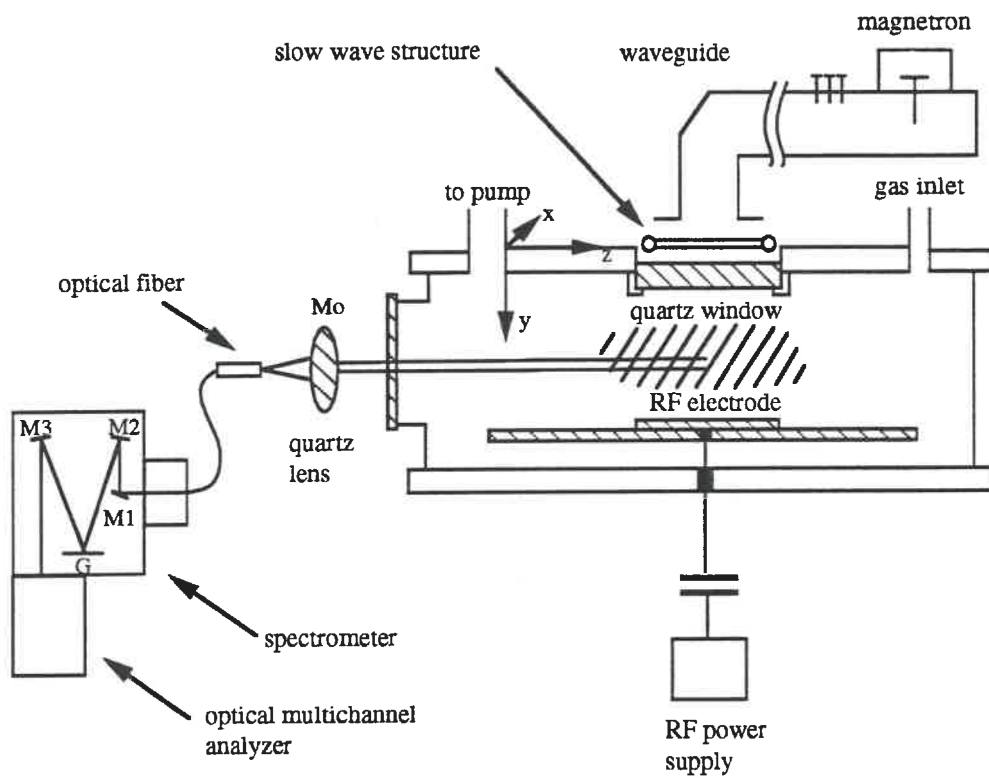

Fig.2.1 Schematic illustration of the experimental apparatus.

electronic mass flow controllers (0 - 100sccm) and the desired pressure, measured by a capacitance manometer, was controlled by an automatic throttling valve.

2.2.Optical Spectrometers

2.2.1.Optical Multichannel Analyzer

Light emitted from the discharge is monitored through a silica window in the reactor wall and recorded using a Princeton Instruments ST120 Optical Multichannel Analyser, with a SPEX 1681C Spectrograph (see Fig.2.1). Emission from the discharge passes through a variable-width vertical slit and a quartz lens (M_o), and it is focused on an optical fiber. In the spectrograph, the light entering through a slit is directed by a 45° mirror M_1 to a collimating mirror (M_2) to the grating (G) and mirror M_3. From here, the spectrum is imaged on the optical multichannel analyser, consisting of an array of 1024 intensified Si diodes. All measurements were recorded and analysed using an AST286 computer. The accessible spectral region of this OES is between 200 and 900nm. The gratings used in this work usually allowed a resolution at 0.5nm, sufficient for most of our studies. In this work a 50x50mm grating (model 3006-500) is employed, having a groove density of 300gr/mm. The central wavelength of light that passes through the spectrometer can be changed by wavelength counter. This operation allows us to scan efficiently over an extended range.

In order to provide spatial resolution, the mirror M_o and optical fiber were mounted on a movable plate placed in front of the plasma chamber window. Micrometrically controlled lateral motion allowed us to sample the plasma at any location between the MW

window and the RF electrode. The spatial resolution of this optical system, limited by the numerical aperture of the optical fiber, was about 6mm.

2.2.2 Vacuum Ultraviolet Spectrometer

The VUV emission spectra were measured using an Acton Research Corporation Model VM-502 Vacuum Monochromator. This instrument, with a focal length of 0.2m, is equipped with a coated grating and mirror. The radiation from the glow discharge is introduced to the entrance slit of the spectrometer through a metal tube without any window. To avoid the effect of VUV absorption in air and in window materials, the spectroscopic system is evacuated independently by a turbomolecular pump. The measurements have been performed in the range 110nm $\leq \lambda \leq$ 400nm, in O_2, Ar, and CH_4 plasmas, with a resolution of 0.4nm. The spectra were plotted using a Houston Instrument, Model 4990 strip chart recorder.

CHAPTER 3

EXPERIMENTAL RESULTS

3.1 The Effect of Actinometric Gases

For every type of plasma, suitable actinometric gases must be used. In order to make an actinometry study of atomic oxygen and atomic hydrogen in the discharges of oxygen and methane, the effects of three actinometers used most often in actinometry, namely Ar, N_2, and He, have been studied in the following section.

3.1.1 Oxygen Plasma

Three different actinometric gases, Ar, N_2, and He, were tested for the study of $[O]_r$ in an O_2 plasma. Figure 3.1 shows the ratios of emission intensities I_o at 844.6nm related to I_{Ar} at 750.4nm, to I_{N2} at 337.1nm, and to I_{He} at 501.6nm in MW, RF, and MW/RF discharges, respectively. In this experiment total pressure p = 0.2Torr, and the flow rates of O_2 and of actinometer gas were 55sccm and 2sccm, respectively.

The emissions come from the plasma center. The actinometric ratios I_o/I_{Ar}, I_o/I_{N2}, and I_o/I_{He} are plotted in figure 3.1(a) as a function of the MW power in the MW discharge. In figure 3.1(b) these ratios are plotted as a function of RF power in the RF discharge, while in the MW/RF discharge (figure 3.1(c)), the three ratios are shown versus the MW power at a constant RF power 150W.

From figure 3.1, one notes that in all cases, the curves of I_o/I_{Ar} and I_o/I_{N2} are very similar, while the trend of I_o/I_{He} is different from the other two curves.

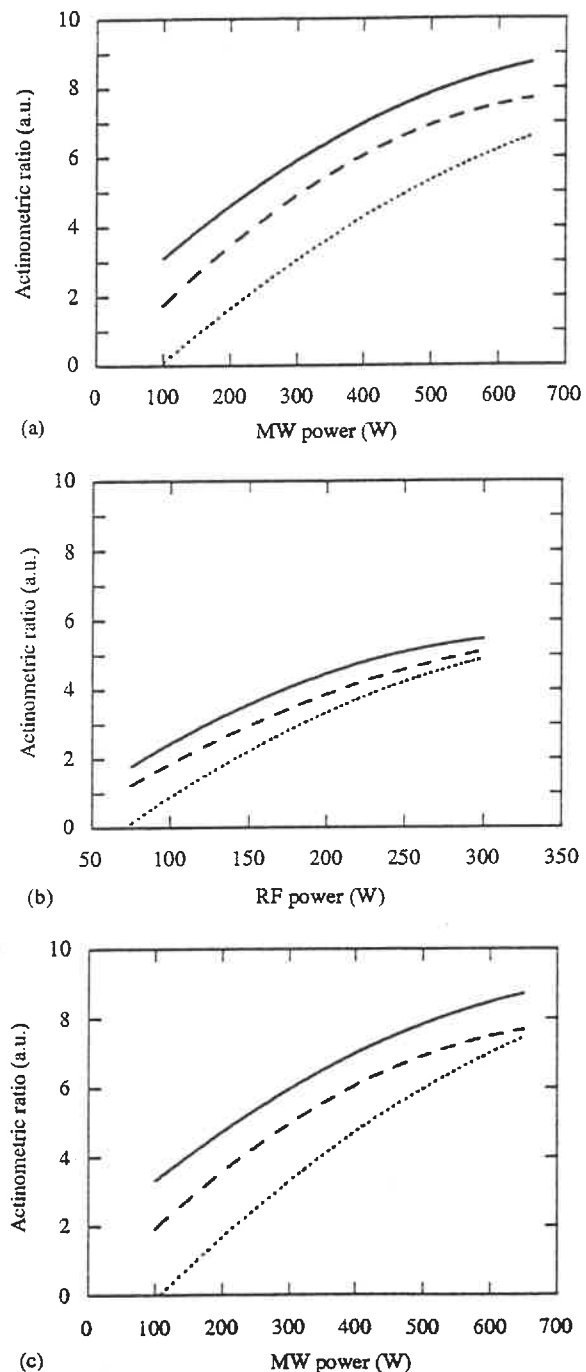

Fig.3.1 Actinometric ratios of I_o at 844.6nm, I_{Ar} at 337.1nm, and I_{He} at 501.6nm as a function (a)MW power; (b)RF power; (c)MW power at a constant RF power 150W. Solid line (—): I_o/I_{Ar}; Dashed line (---): I_o/I_{N2}; and Dotted line (···): I_o/I_{He}. Pressure is 0.2Torr, O_2 flow rate is 55sccm, and total actinometers flow rate is 2sccm.

One restriction for the successful use of actinometry is that the species and the actinometer should have a similar threshold energy of excitation (see section 1.2.1.1). The He line, I_{He} at 501.6nm, which has a high threshold energy of about 23eV, compared to 10.99eV for O, is therefore apparently not suitable to monitor $[O]_r$ in a O_2 discharge. The I_{Ar} and I_{N2} emission lines have thresholds of 13.5eV and 11.1eV, respectively, so they appear to be good actinometers. In the following experiments, Ar is used as the main actinometer since the transition data of the I_{Ar}(750.4nm) line are well known (49).

For reliable use of an actinometer, its addition should not change the properties of the working gas. Therefore, only a small amount of actinometer could be added. To find out the limitation of actinometer addition amount, we perform experiments to examine the effect of Ar addition into the oxygen plasma. The response of the atomic oxygen lines at 844.6nm and at 777.1nm to Ar percentage is plotted in figure 3.2, where the emission intensities from these two lines are seen to remain constant, for $[Ar] \leq 5\%$; following which the oxygen emission decreases. Above 5%, the presence of Ar evidently affects the properties of the O_2 discharge. The experimental result is obtained in MW discharge at a pressure of 0.2Torr and MW power 200W. According to this result, in all subsequent experiments 4% Ar is used to O_2 plasma as actinometer.

3.1.2 Methane Plasma

In order to study of the concentration of atomic hydrogen [H] in the CH_4 plasma using actinometry, 4% of Ar, N_2 and He were added into CH_4 plasma as the actinometers. The relative concentration of atomic hydrogen $[H]_r$ is indicated by using the actinometric ratios of the hydrogen Balmer line H_α (I_H, 656.3nm) to the Ar line (I_{Ar}, 750.4nm), N_2 (I_{N2}, 337.1nm), and He (I_{He}, 501.6nm) (see figure 3.3), respectively. The experiment is

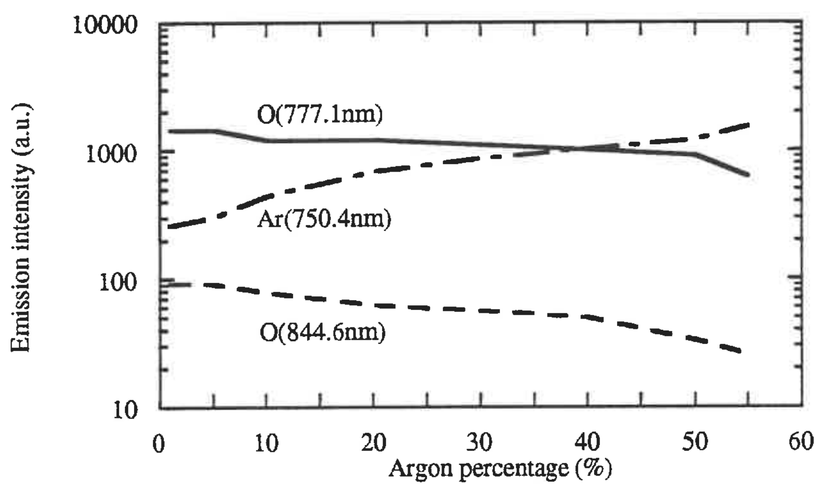

Fig. 3.2 Emission intensities of I_o at 777.1nm and at 844.6nm, and I_{Ar} at 750.4nm as a function of the Ar percentage in the feed in the MW discharge. Total pressure is 0.2Torr, MW power is 200W.

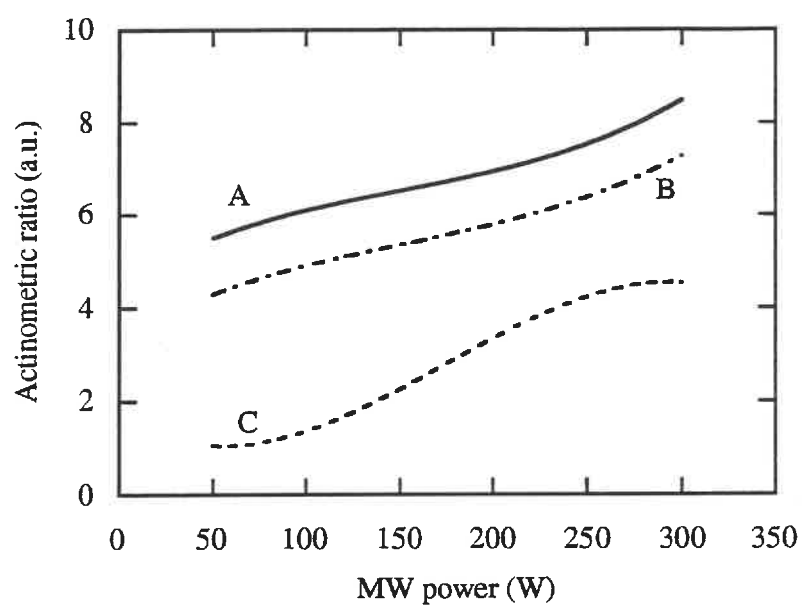

Fig.3.3 Actinometric ratios of I_H at 656.3nm, and I_{Ar} at 750.4nm, I_{N2} at 337.1nm and I_{He} at 501.6nm as a function of MW power in a CH_4 MW plasma at a pressure of 0.2 Torr. Curve A: I_H/I_{Ar} ; CurveB: I_H/I_{N2}; CurveC: I_H/I_{He}.

performed at a constant pressure of 0.2Torr and MW power P_{MW} 150W. While I_H/I_{Ar} and I_H/I_{N2} present similar trends, a remarkable deviation from this behavior can be noticed for I_H/I_{He}. As in section 3.1.1 for O_2, the very high threshold energy of about 23eV causes the actinometric ratio from He (506.1nm) to be unreliable in measuring $[H]_r$, for which the threshold is about 12.08eV. On the other hand, Ar and N_2, whose respective excitation energy thresholds (13.7eV and 11.1eV) are close to that of H_α, are evidently good actinometers for monitoring $[H]_r$ in CH_4 discharges.

The effect of Ar and N_2 actinometer percentage in CH_4 is shown in figures 3.4 and 3.5, respectively. The values of I_H increases when the percentage of Ar or N_2 exceeds 5% in a 150W, 0.2Torr MW plasma, signaling profound changes in the discharge processes. These effects will be discussed in section 4.2.

In the following study of $[H]_r$ in CH_4 plasma, 4% of actinometers Ar (in N_2/CH_4) or N_2 (in Ar/CH_4) are used in MW, RF, and MW/RF discharges.

3.2 Actinometry of Oxygen Discharge

In this section, we study the relative atomic oxygen concentration in the oxygen plasma. We have said that the relation between the optical emission intensity and the species concentration is quite complicated (see section 1.2.1.1). Usually, it is not the emission intensity but the actinometric ratio which varies directly with the species concentration at a constant [Ar]. To see the difference between actinometric ratio, which represents $[O]_r$, and emission intensity, we plotted the O emission line I_o at 844.6nm and actinometric ratio $R_2 = I_o(844.6nm)/I_{Ar}(750.4nm)$ in figure 3.6. Based on the measurements mentioned in the section 3.1.1, 4% Ar has been chosen as the actinometer in this study. The curves obtained here give the variation of I_o at 844.6nm and R_2 as a

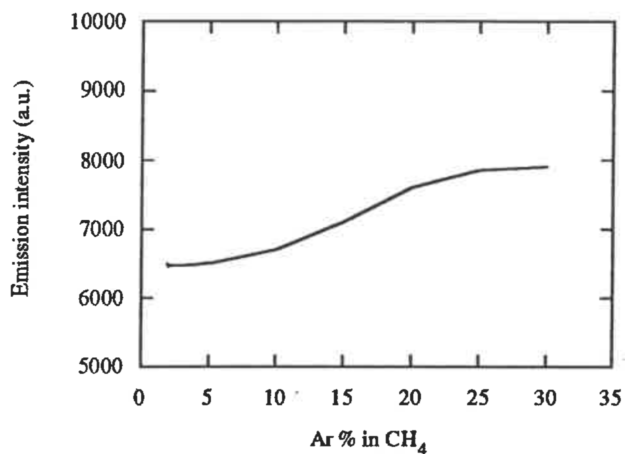

Fig.3.4 Emission intensity of I_H at 656.3nm as a function of Ar percentage in a 0.2Torr CH_4 plasma. MW power is 200W, total flow rate is 57sccm (4% N_2 as an actinometer).

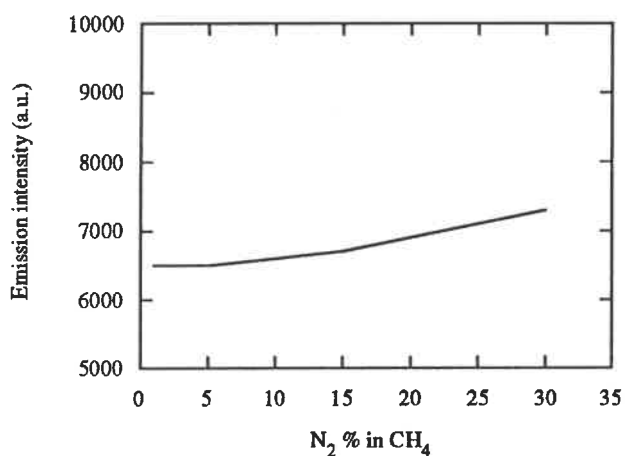

Fig.3.5 Emission intensity of I_H at 656.3nm as a function of N_2 percentage in a 0.2Torr CH_4 plasma. MW power is 200W, total flow rate is 57sccm (4% Ar as an actinometer).

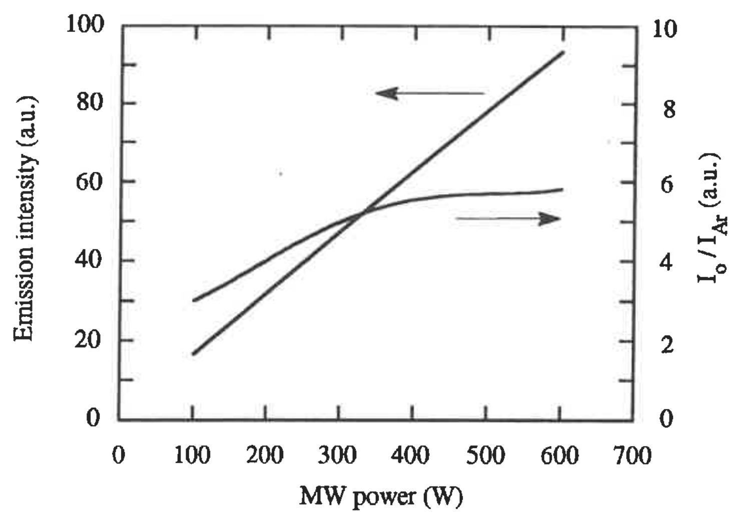

Fig.3.6 Actinometric ratio of I_o at 844.6nm and I_{Ar} at 750.4nm and emission intensity of I_o at 844.6nm line as a function of the MW power in an O_2 plasma. Pressure is 0.2Torr, and total flow rate is 57sccm (4% Ar as an actinometer).

function of MW power in MW discharge at total pressure 0.2Torr, and total flow rate 57sccm. Even though I_o originates from atomic oxygen in the ground state, one notes an obvious difference between the behaviors of I_o and of I_o/I_{Ar}. While I_o increases linearly with MW power, R_2 is found to reach saturation at about 500W. since R_2 represents $[O]_r$, the emission intensity from the atomic oxygen line cannot be used as a measure of $[O]_r$.

Typical emission spectra from MW, RF, and MW/RF discharges in O_2 with 4% Ar are shown in figure 3.7, the observed transitions being summarized in Table 3.1. These spectra originate from the plasma center. In the following studies, two actinometric ratios $R_1 = I_o(777.1nm)/I_{Ar}(750.4nm)$ and $R_2 = I_o(844.6nm)/I_{Ar}(750.4nm)$ will be used to indicate the relative concentration of atomic oxygen $[O]_r$. R_1 and R_2 as a function of plasma parameters including power, spatial position, pressure, and flow rate, have been experimentally investigated.

3.2.1 The Effect of Microwave and RF Power

Figure 3.8 shows how R_1 and R_2 depend on the applied power in three excitation modes, namely MW, RF and MW/RF discharges. The results are obtained at a constant pressure 0.2Torr and flow rate 57sccm (4% of Ar as a actinometer).

In MW discharge (figure 3.8a) the MW power P_{MW} is varied from 100W to 700W. In RF discharge (figure 3.8b) RF power P_{RF} is varied from 100W to 300W. And in MW/RF discharge (figure 3.8c) P_{MW} changes from 100W to 700W at a constant P_{RF} =150W. As shown in figure 3.8, R_1 and R_2 increase when more power is delivered to the discharge; this applies to all three plasma types, namely pure MW (figure 3.8a), RF (figure

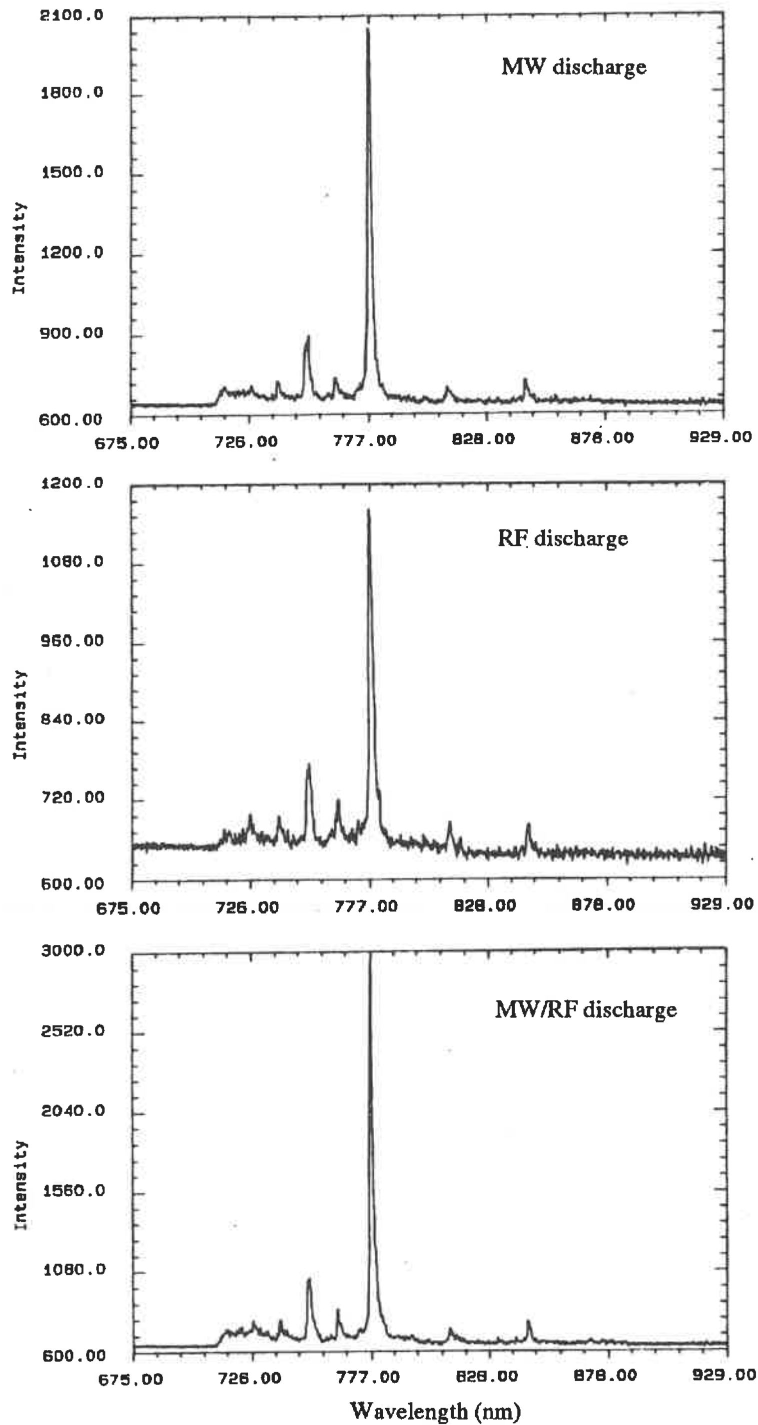

Fig.3.7 Optical emission spectra from the oxygen plasmas under MW, RF, and MW/RF conditions. The pressure is 0.2Toor, flow rate is 57sccm (with 4% Ar as a actinometer).

Table 3.1 Species and transitions in O_2 (4% Ar as an actinometer) glow discharge (Ref.49)

Species	Transition	Wavelength (nm)	Threshold (eV)
O	3p ^5P - 3s ^5S	777.1	10.74
O	3p ^3P - 3s ^3S	844.6	10.99
Ar	4p'[3/2] - 4s [3/2]	738.4	13.298
Ar	4p'[1/2] - 4s'[1/2]	750.4	13.476
Ar	4p [3/2] - 4s [3/2]	763.5	13.168
Ar	4p [3/2] - 4s [3/2]	810.4	13.149

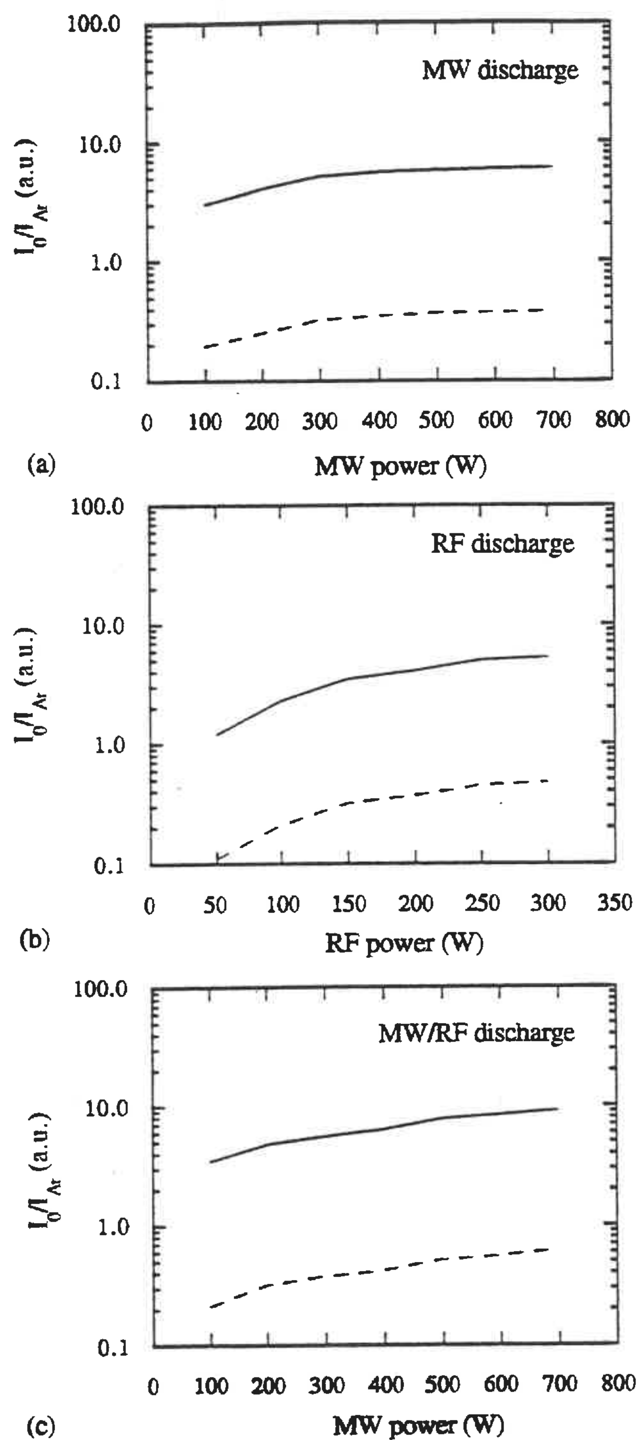

Fig.3.8 The actinometric ratios R_1 (solid line —) and R_2 (dashed line ---) as a function of (a)MW power (b)RF power (c) MW power with a constant RF power 150W. The pressure is 0.2Torr, and total flow rate is 57sccm(4% Ar as an actinometer).

3.8b), and MW/RF (figure 3.8c). As can be seen, the trends of R_1 and R_2 are identical in all cases.

3.2.2 The Effect of Position in the Reactor

In order to explore the spatial variation of emission intensity and $[O]_r$, the experiments are performed at a constant pressure of 0.2Torr and constant power level (P_{MW} = 150W in MW discharge, P_{RF} = 150W in RF discharge, and $P_{MW/RF}$ = 150W/150W in MW/RF discharge).

Typical spectra from O_2/Ar (4%) discharges at different positions are shown in figure 3.9. The dependence of R_1 and R_2 as a function of the axial distance from the MW applicator is shown in figure 3.10. In both cases of the pure MW and RF plasma, emission intensity and values of R_1 and R_2 close to the power applicators (MW or RF) are relatively higher, and decreases with distance (figures 3.10a and 3.10b),while in the MW/RF discharge (figure 3.10c), both emission intensity and R_1 and R_2 exhibit a minimum values at the center. In all cases, higher R_1 and R_2 coincides with stronger emission intensities. The identical trends of R_1 and R_2 are also observed here.

3.2.3 The Effect of Pressure

The oxygen pressure at which the plasma is formed is also important to the production of atomic oxygen. Regarding to the earlier discussion in section 1.2.1.1, the normalized R_1 and R_2 (which are defined as R_1/p_{Ar} and R_2/p_{Ar}, respectively) are used as a measure of $[O]_r$ in pressure dependence studies. The response of actinometric ratios to

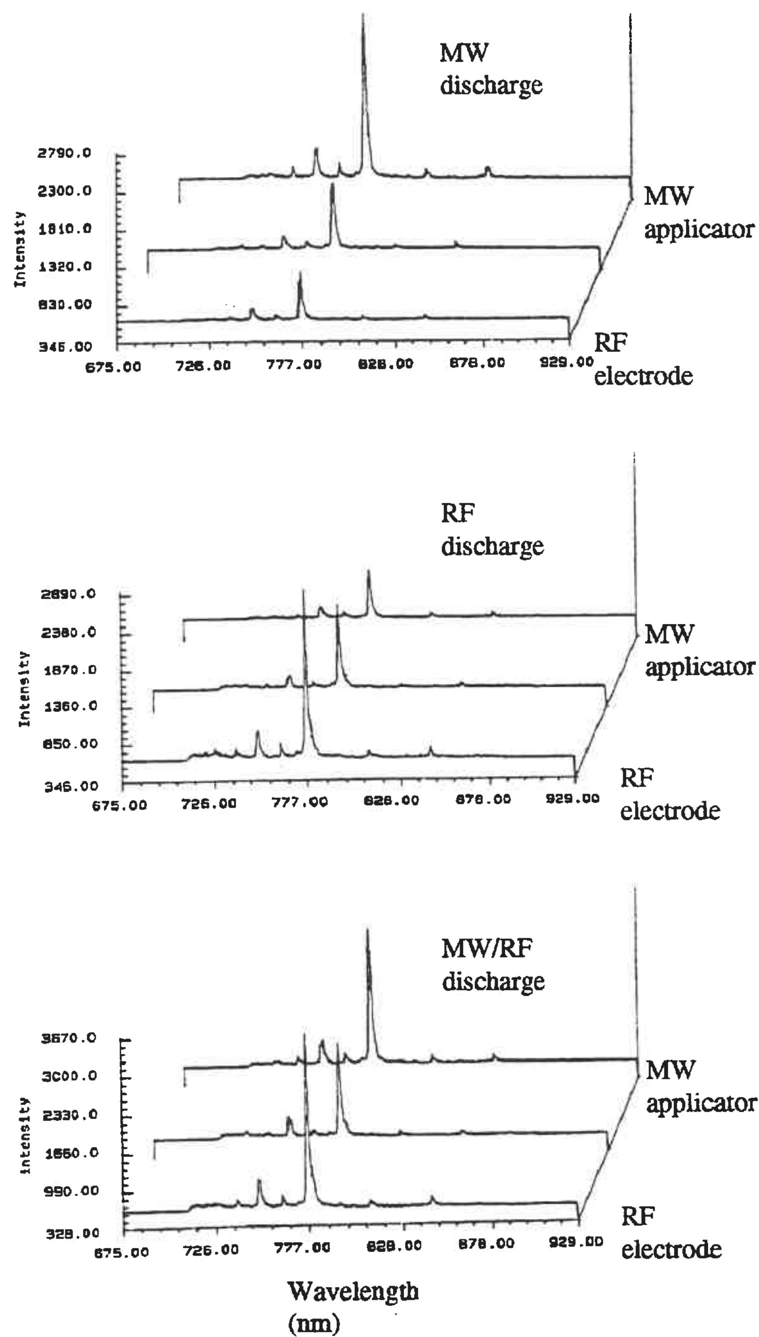

Fig. 3.9 Optical emission spectra from the oxygen discharge under MW, RF, and MW/RF conditions at different locations between the MW applicator and the RF electrode.

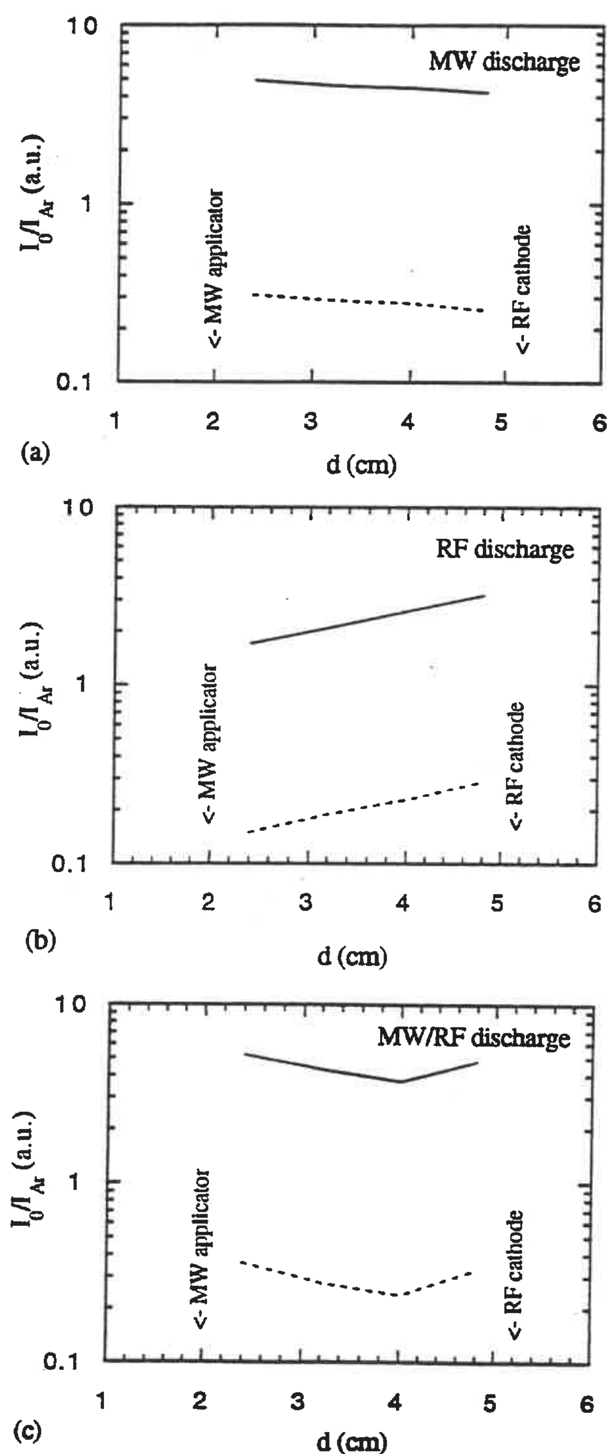

Fig.3.10 Actinometric ratios R_1 (solid line—) and R_2 (dashed line ---) as a function of axial distance from the MW applicator in the O_2 plasma at 0.2Torr. Total flow rate is 57sccm(4% Ar as an actinometer). (a)MW power: 150W (b)RF power: 150W (c)MW/RF: 150W/150W.

oxygen pressure is illustrated in figure 3.11. The experimental results shown there are obtained for a constant power of 150W in MW and RF discharges, and power in MW/RF discharge is $P_{MW/RF}$ =150W/150W. In all excitation modes, R_1 and R_2 increase with O_2 pressure p_{O2}. Here again the curves show that R_1 and R_2 respond to a variation of p_{O2} in the same way.

3.2.4 The Effect of Flow Rate

Another parameter affecting the optimum conditions with respect to the generation of atomic oxygen is the flow rate, at which the working gas is supplied to the plasma zone. Therefore, its effect on $[O]_r$ has also been investigated in our work. As shown in figure 3.12, within the range studied here (50-170sccm) no appreciable changes of R_1 and R_2 have been observed in all cases. This observation indicates that the variation of O_2 flow rate has not significant effect on $[O]_r$ in this range. Similar to the above observations, identical trends of R_1 and R_2 are also found here.

3.3 Actinometry of Methane Discharge

In this section, we study the atomic hydrogen concentration in the methane plasma. Typical emission spectra from a CH_4 discharges are presented in figure 3.13. The emission lines are identified in table 3.2 and summarized together with the threshold energies. First of all, let us examine the behavior of $[H]_r$ in the Ar/CH_4 plasma. The effect of Ar percentage on $[H]_r$ in this plasma becomes clear when we plot the graph shown in

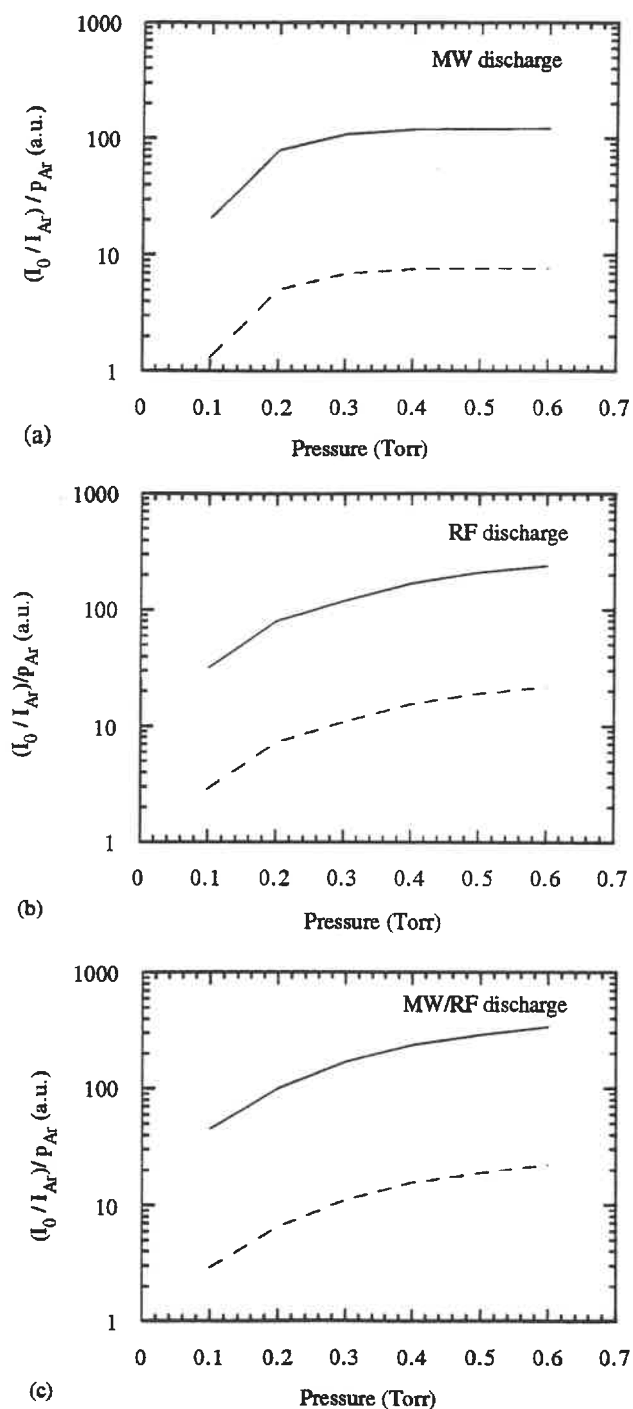

Fig.3.11 Normalized actinometric ratios R_1/p_{Ar} (solid line —) and R_2/p_{Ar} (dashed line ---) as a function of O_2 pressure. The flow rates of O_2 and Ar are 55sccm and 2sccm, respectively. (a)MW power: 150W (b)RF power: 150W (c)MW/RF: 150W/150W.

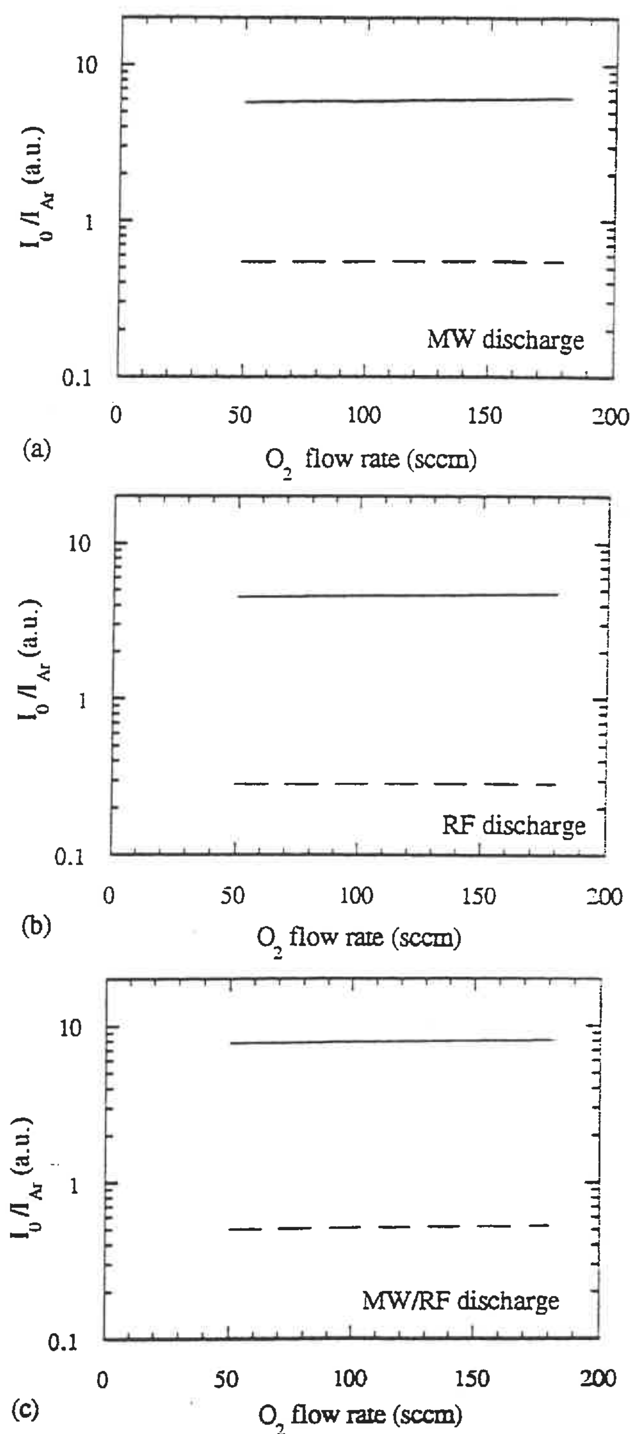

Fig.3.12 Actinometric ratios R_1 (solid line—) and R_2 (dashed line ---) in the vicinity of the RF electrode as a function of O_2 flow rate. The pressure is 0.2Torr with 2sccm of Ar as an actinometer. (a) MW power: 150W (b) RF power: 150W (c)MW/RF: 150W/150W.

figure 3.14, where N_2 (4%) is used as an actinometer. $[H]_r$ is characterized by the actinometric ratio $R_3 = I_H(656.3nm)/I_{N2}(337.1nm)$ in this experiment at a pressure of 0.2Torr. It can be seen in this figure that R_3 increases when more Ar is added up to 30% in all three excitation discharge modes, namely MW, RF, and MW/RF. P_{MW} is 150W in MW discharge and P_{RF} is 150W in RF discharge. For the MW/RF discharge, both P_{MW} and P_{RF} are 150W.

Next, we examine the behavior of $[H]_r$ in the N_2/CH_4 plasma at same condition as in the above experiment. A similar situation is observed when N_2 is added to the CH_4 feed gas and 4% Ar is used as an actinometer (see figure 3.15), namely, higher N_2 concentration contributes to enhanced actinometric ratio $R_4 = I_H(656.3nm)/I_{Ar}(750.4nm)$, which is used to characterize $[H]_r$ in this experiment.

From the above experimental results, the following conclusion can be reached: the relative concentration of atomic hydrogen $[H]_r$, which is respectively represented by R_3 and R_4, can be enhanced by the addition of Ar or N_2 into the CH_4 plasma.

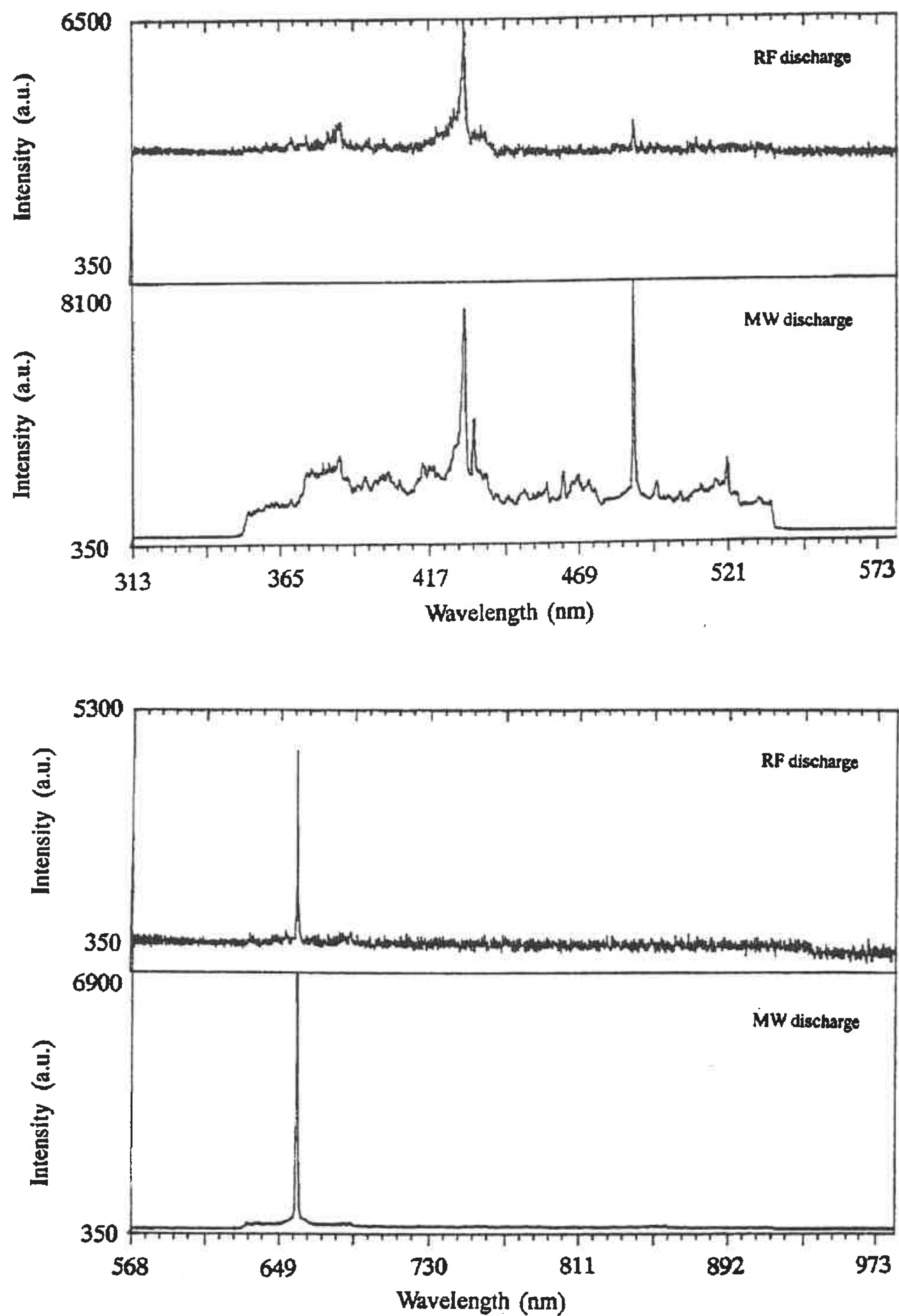

Fig.3.13 Optical emission spectra for methane in the MW and the RF discharges.

Table 3.2 Species and transitions in CH_4 glow discharge (Ref.49)

Species	Transition	Wavelength (nm)	Threshold (eV)
CH	$B^2\Sigma \rightarrow X^2\Pi$	387.1	3.21
CH	$B^2\Sigma \rightarrow X^2\Pi$	388.9	2.87
CH	$A^2\Delta \rightarrow X^2\Pi$	431.4	3.18
CH	$A^2\Delta \rightarrow X^2\Pi$	438.5	
CH+	$A'\Pi \rightarrow X^2\Sigma$	422.5	2.99
C_3		405.0	
C_2	Swan	473.7	
C_2	Swan	516.5	2.48
H_β	Balmer	486.1	12.74
H_α	Balmer	656.3	12.08

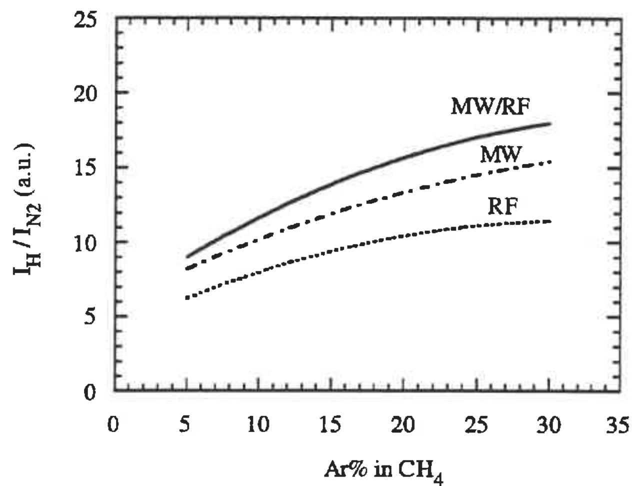

Fig.3.14 Actinometric ratio I_H/I_{N2} as a function of the Ar percentage added to the CH_4 in MW, RF, and MW/RF plasmas (4% N_2 as an actinometer).

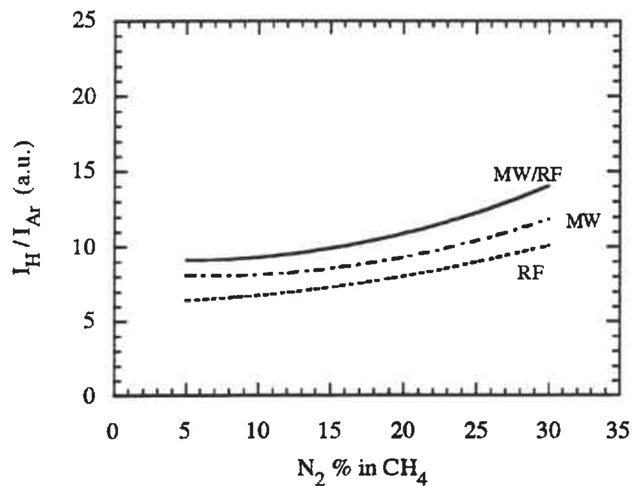

Fig.3.15 Actinometric ratio I_H/I_{Ar} as a function of the N_2 percentage added to the CH_4 in MW, RF, and MW/RF plasmas (4% Ar as an actinometer).

CHAPTER 4

DISCUSSION

4.1 Oxygen Plasma

Before we discuss individually the results in Chapter 3, let us consider some fundamental processes in an oxygen discharge.

Consider first the formation of atomic oxygen. In a low-pressure oxygen discharge, the main processes giving rise to the formation of atomic oxygen are electron-impact dissociation and electron-excited dissociation (1):

$$e + O_2 \dashrightarrow O + O + e \quad (8)$$

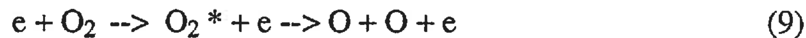

$$e + O_2 \dashrightarrow O_2{}^* + e \dashrightarrow O + O + e \quad (9)$$

The cross sections of processes for electron-impact dissociation (equation.8) and excited-dissociation (equation.9) are 2.25 x 10^{-18} cm^2 and 3 x 10^{-20} cm^2, respectively (1). Since the cross section means the probability of a process, the process described by equation (8) is the dominating process. Therefore, we assume that most of atomic oxygen arises from the electron-impact dissociation.

Secondly, let us consider the recombination process of atomic oxygen. The loss of atomic oxygen in the discharge proceeds via both homogeneous and heterogeneous processes, namely volume recombination and wall recombination; respectively (1):

$$O + O_{\,volume} \dashrightarrow O_2 \quad (10)$$

$$O + O_{\,wall} \dashrightarrow O_2 \quad (11)$$

The rate constants for processes (10) and (11) are respectively characterized by the volume and wall recombination coefficient K_v and γ.

The third key process is excitation. The main excitation channels for optical emission from a low-pressure oxygen plasma are (37):

$$e + O\,(\text{ground}) \dashrightarrow O^*\ (\text{excited state}) + e \qquad (12)$$

$$e + O_2 \dashrightarrow O^* + O + e \qquad (13)$$

where equations (12) and (13) describe electron-impact excitation and dissociative excitation, respectively. The cross sections of these two processes depend on the particular emission frequency and on the electron energy. For the 777.1nm ad 844.6nm oxygen emission lines used most often in the actinometric technique, their maximum cross sections for electron-impact excitation are about one order of magnitude larger than those for dissociative excitation (37). Consequently, we can assume that these two emission lines arise from the process described by equation (12) (i.e. electron-impact excitation).

The principal results of the actinometric study of the oxygen discharge presented in Chapter 3, can be summarized as follows:

(i) Trends in the actinometric ratios $R_1 = I_o(777.1\text{nm})/I_{Ar}(750.4\text{nm})$ and $R_2 = I_o(844.6\text{nm})/I_{Ar}\,(750.4\text{nm})$ have been found to be identical. They can be used as a measure of relative concentration of atomic oxygen $[O]_r$;

(ii) The actinometric ratios R_1 and R_2 increase with raising the power delivered to the discharge, but the behaviors differ for the MW, RF, and MW/RF plasma excitation modes;

(iii) For each of the excitation modes, R_1 and R_2 display a distinct spatial position dependence in the interelectrode region;

(iv) The values of R_1 and R_2 increase monotonically with the oxygen pressure for each of the three modes.

In the following, our experimental results will be compared with the data published by other authors, and they will be discussed in the terms of the above-mentioned

processes, namely dissociation, recombination, and excitation under various experimental conditions.

4.1.1 The Effect of Power Density

In this section, we will discuss our experimental results of power density dependence and compare them with those reported by others.

Various plasma systems generally differ due to their design, and therefore direct comparison of the effect of individual variables is very difficult. To be able to evaluate the trend of the effect of electric power it is convenient to use the power density, a parameter defined here as the total power divided by volume of plasma.

To assure a reliable measurement, both actinometric ratios R_1 and R_2 are used in our work, and in all experiments, since both of them exhibit identical trends. Because R_2 is mostly used by others, we choose this quantity in the following discussion.

In figure 4.1, we compare our actinometric ratio R_2 from figure 3.1 with experimental results of Safari (44) for a MW cavity system, and of Amorim et al. (38) for a DC tubular system. We also show in this figure the dissociation degree Y (=$[O]/2[O_2]$) determined by Bosisio et al. (50) in a large volume MW system, by Mearns et al. (51) in a MW cavity system, and by Amorim et al. (38) in a DC system.

As mentioned in section 1.2.1, equation (6) defined the relation between R_2 and the concentration of atomic oxygen [O]:

$$[O] \propto [I_o(844.6nm)/I_{Ar}(750.4nm)]\ [Ar] \qquad (14)$$

i.e. $$[O] \propto R_2\ [Ar] \qquad (15)$$

Since the numerical value of the proportionality constant in this relation is unavailable, the actinometric technique cannot provide the absolute value of [O]. We can only say that [O] varies directly as R_2 at a constant [Ar], but we cannot determine its numerical value. This is

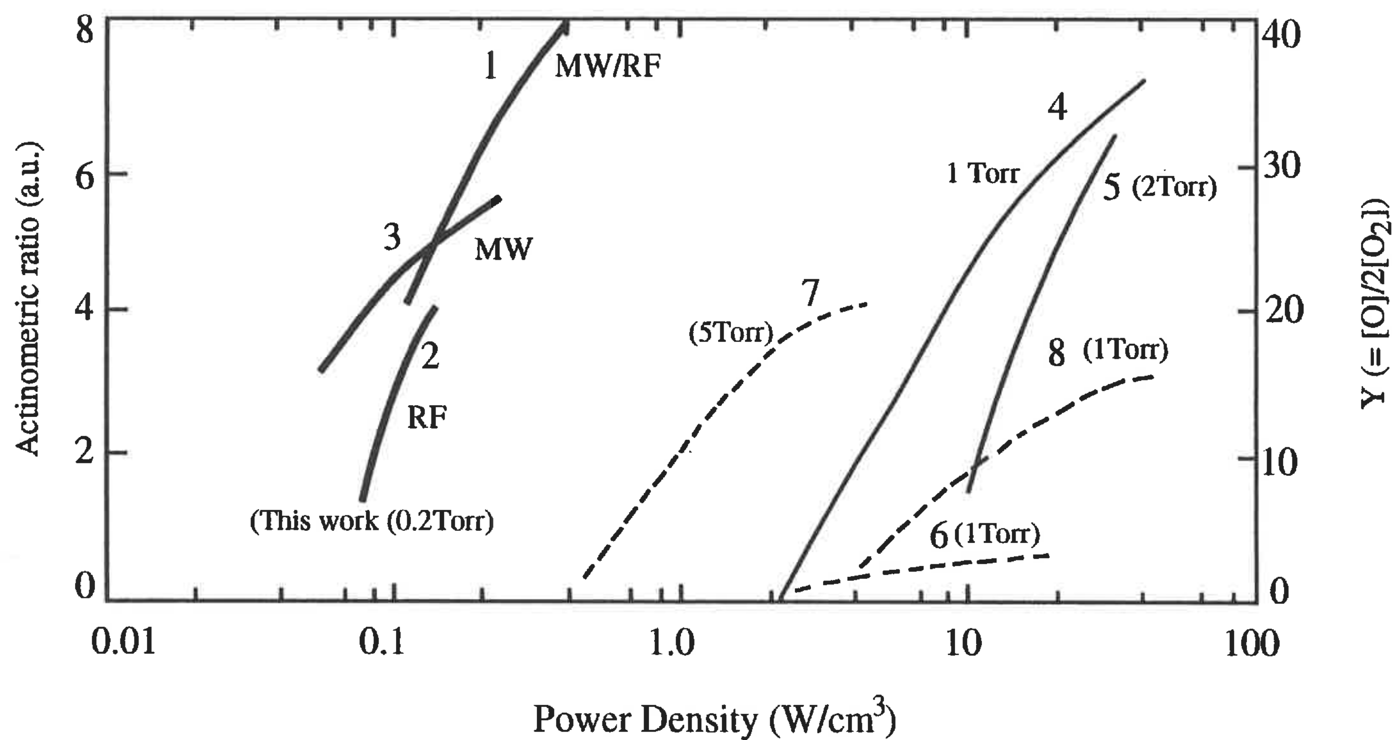

Fig.4.1 Actinometric ratios (solid line —) and dissociation degree Y (dashed line (----) as a function of power density: our data from fig.3.8 (curves 1, 2, and 3); Amorim et al. (41) (curves 4 and 6), Safari (55) (curve 5), Bosisio et al. (59) (curve 7), Mearns et al. (56) (curve 8). In all actinometric ratios, O-844.6nm was used; and Ar-750.4nm is used in curves 1-4 but Ar-811.5nm in curve 5.

the reason for that we can only get the relative concentration of atomic oxygen $[O]_r$ from this relation.

Now, we start to discuss our results of R_2 from figure 4.1. We see that the curves of R_2 in our MW/RF (curve 1), RF (curve 2), and MW (curve 3). discharges present different behaviors. R_2(MW) (curve 3) is higher than its RF counterpart R_2(RF) (curve 2) at the same power density. To explain this observation, let us go back to the equations (8) and (9), which describe the formation processes of atomic oxygen. The result suggests that the electron density in MW plasma being higher (collisions occur more frequently), this higher value of electron density n_e results in higher $[O]_r$. Since the value of n_e in a MW discharge is larger compared to an RF discharge at same power density (9), $[O]_r$ in the MW discharge is higher than that in RF discharge. This means that the MW discharge is more efficient in the formation of atomic oxygen compared with RF discharge.

The situation is more complicated when the MW and the RF discharge are applied simultaneously. In the data shown in figure 4.1 for the MW/RF discharge (curve 1), RF power was kept constant at 150W, and the MW power was increased from 50 to 700W. The curve in figure 4.1 shows what occurs when we increase power density by adjusting MW power at constant RF power: R_2(MW/RF) rises with power density. This is because also n_e rises with power density and so does $[O]_r$. When we compare the slopes of R_2(MW/RF) with that of R_2(MW) or R_2(RF), we can see the more rapid increasing in R_2(MW/RF). This is correlated with the higher etch rate of polyimide in the MW/RF oxygen plasma (52). In earlier discussion, we have said that the electron density n_e would affect the value of R_2, and we also know that the value of R_2 in the MW discharge is higher than that in the RF discharge at same power density. However, if we want to compare R_2 in different discharge modes, the knowledge of n_e as a function of power density in these three discharge modes is needed. The ion flux in the MW/RF discharge has been measured in this laboratory (19). Its value is found to be higher than that in the MW discharge at

fixed power. But the variation of n_e at various power density values in these three discharge modes is nor known and further study in this subject is suggested.

We know that R_2 is an indirect measure of [O], and represents its relative values $[O]_r$. The direct way to test if R_2 is consistent with the real behavior of [O] is to measure the absolute value of [O]. If we find that the trend of R_2 is consistent with [O] from the absolute measurement, we would then naturally think it is correct. To determine the absolute value of [O], VUV and titration measurements can be employed. More details about these techniques are described in section 1.2.1.2. However, the measurements could not be performed in our laboratory.

On the other hand, we can confirm the reliability of our results by comparison of R_2 with actinometric results of Amorim et al. (38) (curve 4 in figure 4.1) and Safari (44) (curve 5 in figure 4.1); their results have been confirmed by VUV measurement. From figure 4.1, it can be seen that our results exhibit a similar trend as those observed by them for different discharge modes and geometries: with increasing power density, the actinometric ratio rises. In agreement with the results confirmed by the VUV measurement, our result should be reliable.

With the aid of the behavior of dissociation degree Y of molecular oxygen, we can see another evidence of this reliability. The studies of Y have been performed by Amorim et al. (38) (curve 6), by Bosisio et al. (50) (curve 7), and by Mearns et al. (51) (curve 8). From figure 4.1, it can be seen that Y determined by them presents comparable behavior with the trend of our actinometric ratio: Y rises with the power density. Notice that Y is defined as $[O]/2[O_2]$. The increasing of Y indicates us that [O] rises directly with power density. This agrees with our observation again.

4.1.2 The Effect of Position in the Reactor

The axial profiles of both the emission intensity (figure 3.9) and the actinometric ratio (figure 3.10) reveal spatial variation for MW, RF, and MW/RF discharges. To understand our observations let us now consider the dissociation and the excitation described by equations (8), (9), (12), and (13). We can find that all these processes are caused by the electron collisions with atomic and molecular oxygen. In the plasma, it is electric field **E** (defined as the electric force field on one positive elementary charge) which accelerates the electrons. In the region where **E** is stronger, the electrons move faster and collide with species more frequently. Thus, the collision would break apart the molecular oxygen effectively; and also excite atomic and molecular oxygen more often. Consequently, the emission intensity and $[O]_r$ should be high in the region of high **E** values.

From above discussion, we can find that the **E** is very important to the dissociation and excitation processes. Finding a reasonable explanation for our observations is related to the spatial variation of **E** in MW, RF, and MW/RF discharges. To find the complete shape of **E** is more complicated, but we can only approximate its distribution in the axial direction based on previous studies by others: according to Bosisio et al. (50), the highest value of **E** in the MW discharge appears near the MW window, and its magnitude falls with the axial distance d. The distribution of **E** in the RF discharge was studied by Oelrich-Hill et al. (53), and also by Haverlag et al. (54). Their investigations point out that the higher value of **E** is located in front of RF cathode. Considering that **E** in MW/RF discharge is determined by the combination of that of MW and RF, it is not hard to understand that its higher values should be located near both the MW window and the RF cathode.

As we already mentioned, the stronger **E** would cause high emission intensity and efficient dissociation. This is the reason for that the highest values of the emission intensity and the actinometric ratio are located near the MW window and RF cathode in all cases.

In summary, then, when **E** in MW, RF, and MW/RF discharges along with the axial direction is not uniform, we observe that both emission intensity and actinometric ratios R_1 and R_2 are spatially non-uniform in this direction. The maximum values of them in all excitation modes are corresponding to the higher values of **E**.

4.1.3 The Effect of Oxygen Pressure

Now we examine the dependence of actinometric ratio on the oxygen pressure p_{O2}. According to Coburn and Chen (33), the normalized actinometric ratio to the actinometer's partial pressure (i.e. p_{Ar} in our case) should be used as a measure of $[O]_r$ in a pressure dependence study. In our case, we use the normalized values of R_1 and R_2 (i.e. R_1 and R_2 divided by p_{Ar}) to indicate $[O]_r$. Just as O-844.6nm is most often used by others, we choose normalized R_2 in the following comparison. Figure 4.2 shows the effect of p_{O2} on normalized R_2 in our work; and also the actinometric ratios of Booth et al.(45), Joubert et al. (12), and Safari (44). O-844.6nm is used by all these authors; expect that Safari used Ar-811.5nm instead of Ar-750.4nm in his actinometric ratio. It can be seen that the value of actinometric ratios increase with p_{O2} in all cases. Our data (curves 1, 2, and 3), which cover the pressure range from 0.1 to 0.6Torr, correspond qualitatively to the actinometric ratios of Joubert et al. (12) (curve 4) for an ECR system from 10^{-4} to 2×10^{-4} Torr, and of Safari (44) (curve 7) for a MW cavity system at pressures between 1 to 4 Torr.

To examine the effect of p_{O2} on $[O]_r$, it is useful to examine equations (12) and (13), which described the formation processes of atomic oxygen in an oxygen plasma. It is

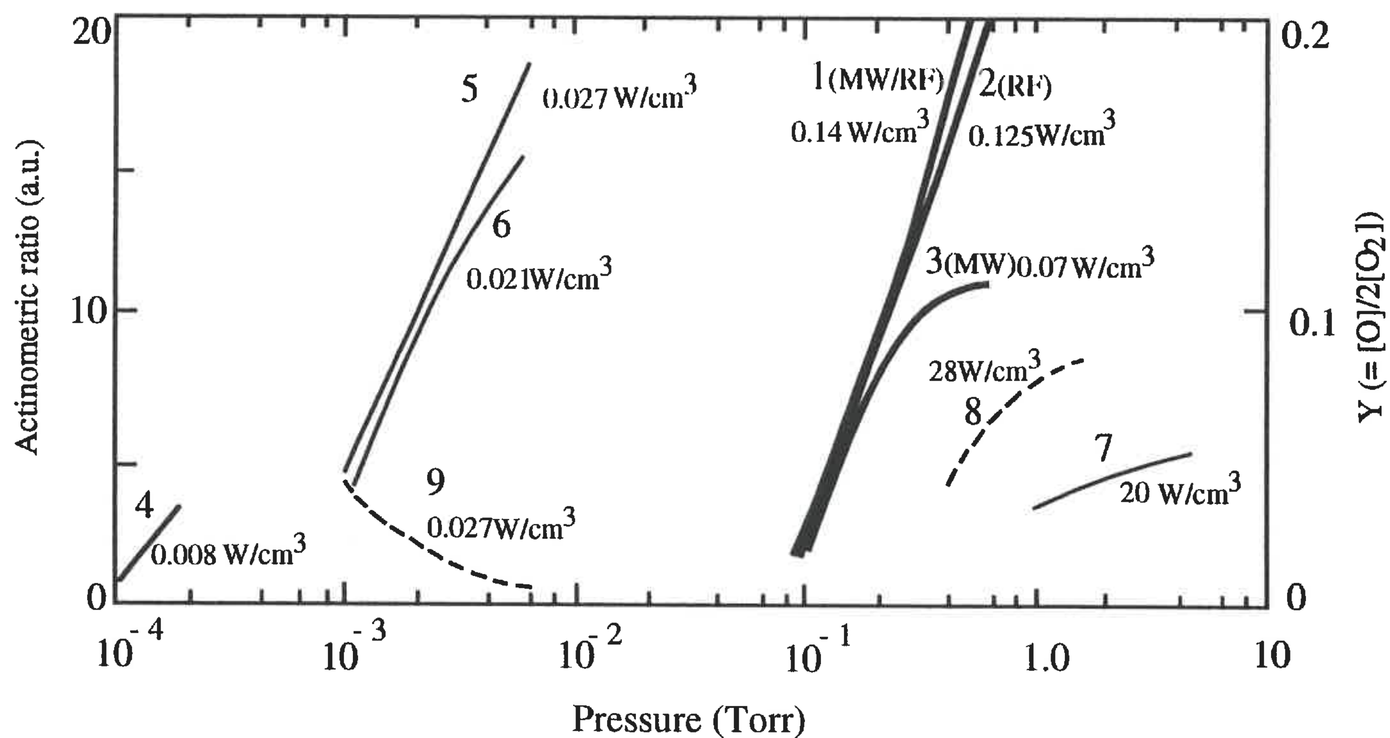

Fig.4.2 Actinometric ratios (solid line —) and dissociation degree Y (dashed line ----) as a function of pressure: our data from fig.3.12 (curves 1, 2, and 3, data multiplied by 0.1); data from Joubert et al. (15) (curve 4), from Booth et al. (61) (curves 5, 6, and 9), from Safari (55) (curve 7), and from Kaufman (57) (curve 8). In the actinometric ratios, O-844.6nm was used in all curves; and Ar-750.4nm was used in curves 1-6 but Ar-811.5nm in curve 7.

easy to recognize that the formation of atomic oxygen is also affected by the concentration of molecular oxygen $[O_2]$ in the chamber. Since raising $[O_2]$ also raises the occurrence of formation processes of atomic oxygen. The concentration of atomic oxygen [O] is then enhanced. $[O_2]$ must rise if p_{O2} increases (this is Boyle's law). So we can say that [O] should increase with p_{O2}. Therefore, the rising of normalized actinometric ratio, which represents $[O]_r$, with p_{O2} is reasonable. It can be seen that the trends of R_2 in the three discharge modes (i.e. the slopes of Curves 1, 2, and 3) agree with the power density dependence at fixed pressure. The higher power density causes the rapid increasing of $[O]_r$. Since the measurements are performed at a constant power density, the values of $[O]_r$. cannot increase without limit: saturation is indeed observed in the MW discharge (curve 3) due to its lower power density.

The data of dissociation degree Y (= $[O]/2[O_2]$) from Kaufman (55) fits well with our results. It follows his experiments (curve 8) that Y increases with raising p_{O2}. Since the higher value of Y means higher [O] (we can understand this point from above definition of Y). This agrees also with our results.

Using actinometric ratio as a measure of $[O]_r$ cannot be extended to all experimental conditions. An example is the experiment of Booth et al.(45) (see curves 5 and 6 in figure 4.2). In their ECR system using a pure oxygen discharge at pressures from 0.001 to 0.006 Torr, the actinometric ratios are found poorly correlated with [O] as determined from VUV measurements. In fact, their Y data (see curve 9) show a decrease with pressure, in contrast to the above-mentioned results of Safari. The real reason why the actinometric ratio fails in their case is not very clear. One possible explanation is that the motion of electrons in an ECR system is different from a MW cavity system (44). The behavior of electrons due to the external magnetic field in an ECR system is more complex; and it depends on the distribution of the electric and magnetic fields in the plasma chamber, which has not been discussed by the authors in any more detail.

So far we have discussed the effect of oxygen pressure p_{O2} on the formation processes of atomic oxygen. We found that the normalized R_2 values rise with p_{O2}, since an enhanced pressure can accelerate the dissociation processes(see equations (8) and (9)). Our results can be confirmed by the observation by Kaufman. His data for Y agree with our results.

p_{O2} will affect the recombination processes: at high pressure the recombination processes become faster due to the rising collision frequency. Thus, the loss rate of atomic oxygen rises with p_{O2}. The two most likely recombination process of atomic oxygen are given by equations (10) and (11). In general, it is difficult to ascertain which one of equations (10) and (11) is most important. One of the reasons is that the coefficient rate K_v of equation (10) strongly depends on the experimental conditions, and γ of equation (11) depends on the material of the wall. The literature (1, 55, 56) shows that K_v lies scattered in the region from 4.5×10^7 to 3.2×10^{15} mole^{-2} cm^6 sec^{-1}; and γ is from 10^{-5} to 10^{-2}sec^{-1} for silica. No γ values of stainless steel and aluminum (used in our case) could be found. For this reason, we cannot give a quantitative estimation about the recombination of atomic oxygen. In our large volume discharge system, the volume recombination process should be more important compared with that in a long tube system, where the wall recombination process is the main recombination process. Further study in this field would be useful.

4.1.4 The Validity of Actinometric Results

The key assumption involved in the actinometric technique is that the dominating excitation channel for main species (atomic O in our case) and actinometer is electron-impact excitation. This means that only if R_1 and R_2 arise from equation (12), they can be used as a good measure of $[O]_r$.

In the following discussion we first focus our attention on the general excitation mechanism of the actinometric ratio $R(= I_o/I_{Ar})$; then we will discuss the special conditions for R_1 and R_2.

In general, the main excitation channels in an oxygen plasma are given by equations (12) and (13). Usually, both these processes contribute to the actinometric ratio R (61):

$$R = I_o/I_{Ar} = C[O]/[Ar] + C'[O_2]/[Ar] \qquad (16)$$

where the first term on the right represents the contribution from electron-impact excitation of atomic oxygen, and the second term represents the contribution from dissociative excitation of molecular oxygen. Since the actinometric technique is valid only if R arises from electron-impact excitation, it can only be used when the dissociative excitation process is negligible. This is the principal limitation of the actinometric technique.

In the following we will examine whether the process of dissociative excitation can be neglected for our actinometric ratios R_1 and R_2. The values of R_1 and R_2 are determined from O-777.1nm, O-844.6nm, and Ar-750.4nm lines intensities, respectively. The Ar-750.4nm arises from electron-impact excitation (36). So to find out if O-777.1nm and O-844.6nm also come from the same process, one can compare the cross section for dissociative excitation with that of electron-impact excitation. If the former one is smaller compared with the latter one, the corresponding process can be neglected. Figure 4.3 shows the cross sections of these two lines. We can note that the cross sections of electron-impact excitation for O-777.1nm and O-844.6nm are much larger than that of dissociative excitation, in particular at low electron energy level (<20eV). For our low-pressure plasma, the average electron energy is less than 20eV. Since all lines involving R_1 and R_2, namely Ar-750.4nm, O-777.1nm, and O-844.6nm, originate from electron-impact excitation, of course, R_1 and R_2 should also arise from this process and both R_1 and R_2 provide reliable measurements of $[O]_r$.

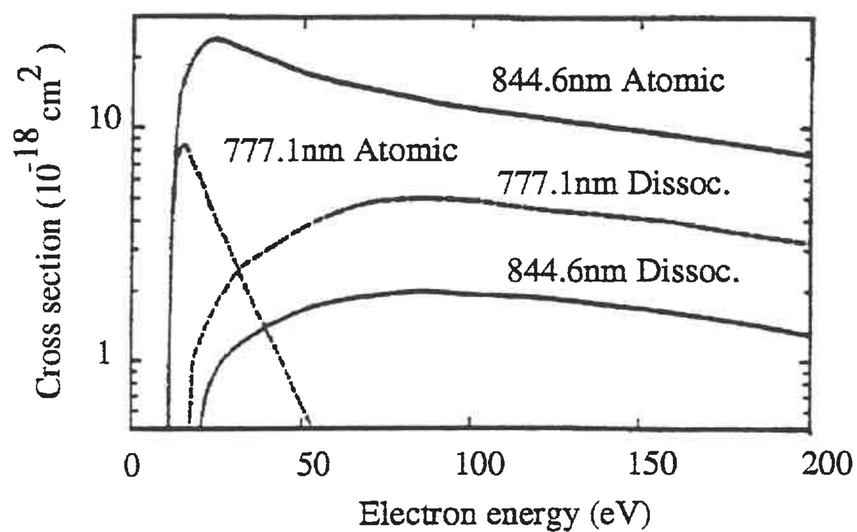

Fig.4.3 Cross sections for electron impact excitation and dissociation are shown as a function of electron energy (data after Walkup et al. (37)).

Several previous studies (40,41,55) agree with this conclusion. For instance, Amorim et al. (41) tested the validity of R_1 and R_2 as a measure of $[O]_r$ by using VUV measurement. Their result shows that the trends of both R_1 and R_2 are well correlated with that of [O] obtained from VUV measurement.

We summarize, then, the whole situation as follows: to estimate the concentration of atomic oxygen [O], we use actinometric ratios R_1 and R_2 as a measure of $[O]_r$. We assume that both of R_1 and R_2 are mainly determined by the electron-impact excitation. This assumption is reasonable in theory, and it has been well tested in several previous experiments. Since it can be relied upon, our results are reliable. Identical trends of R_1 and R_2 show that each ratio can be used independently as a measure of $[O]_r$.

4.2 Methane Plasma

We shall now discuss our results for atomic hydrogen concentration in methane plasma, which is determined by the actinometric ratios R_3 ($=I_H(656.3nm)/I_{N2}(337.1nm)$) or R_4 ($=I_H(636.5nm)/I_{Ar}(750.4nm)$), respectively.

Let us begin with the results shown in figure 3.16 where we plot R_3, which is used as a measure of $[H]_r$ in Ar/CH_4 plasma. Here N_2 is used as an actinometer. It can be seen that R_3 rises with the percentage of Ar in all excitation modes, i.e.[H] increases.

Now, we will examine the role of argon in CH_4 plasma. Argon, with no rotational or vibrational degrees of freedom, can only be excited by electrons with sufficient energy. Its first excited state is 11.5eV. In Ar/CH_4 plasmas, the energy transferred from metastable argon to methane is sufficient to cause several bonds to break. The following channels are open to dissipate 11.5eV (62):

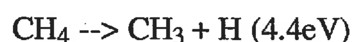

$$CH_4 \dashrightarrow CH_3 + H \ (4.4eV)$$

$\rightarrow CH_2 + H_2$ (4.8eV)

$\rightarrow C + 2H_2$ (8.0eV)

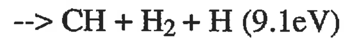
$\rightarrow CH + H_2 + H$ (9.1eV)

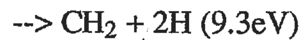
$\rightarrow CH_2 + 2H$ (9.3eV)

The molecular hydrogen can also be dissociated by the electron-impact process. Therefore, argon enhances $[H]_r$ in the methane plasma due to above dissociation processes. Some experimental results fit with this conclusion (2,62). For instance, the previous work in this laboratory (2) on Ar/CH_4 plasma used for a C:H film deposition shows that more DLC characteristics are observed when Ar is added to CH_4. This is due to the presence of atomic H which favors the formation of sp^3 type of bonding by a enhanced etch removal of the sp^2 hybridization. This is further confirmed by infra-red spectroscopy. The experimental result therefore confirm a rise in $[H]_r$.

Now, let us examine what happens when N_2 is added into CH_4 plasma. here, Ar is used as an actinometer. Figure 3.17 shows that R_4, which is used as a measure of $[H]_r$ in N_2/CH_4 plasma, increases when more N_2 is added. This is because that N_2 can involve several machanisms of [H] generation by the following reactions (63):

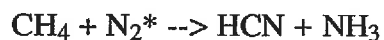
$CH_4 + N_2^* \rightarrow HCN + NH_3$

$CH_4 + N \rightarrow HCN + H_2 + H$

$CH_3 + N \rightarrow HCN + H_2$ (or 2H)

$CH_4 + H \rightarrow CH_3 + H_2$ (or 2H)

These results show that N_2 and N also have an effect on the H atom concentration in the N_2/CH_4 plasma.

The above results indicate that the decomposition of methane is promoted when Ar or N_2 are added. This is associated with the energy transfer processes from species added to methane. Similar trends are observed for all three types of plasma, MW, RF, and

MW/RF. Here, we also should note that $[H]_r$ would tend to saturate when adding more Ar or N_2 due to the fixed power density and a constant pressure.

CHAPTER 5

CONCLUSION

In the present work the actinometric technique has been used for the analysis of low pressure plasma. The set-up employed allows to perform measurements in three types of discharge modes, namely MW, RF, and MW/RF. The optical multichannel analyzer, equipped for spatial resolution, is used to monitor the optical emission spectra from these three excitation modes. The suitable actinometric ratios are used as a measure of the relative concentrations of the main species, namely $[O]_r$ and $[H]_r$, particularly under conditions used in etching (oxygen plasma) and deposition (methane plasma).

In the first part of this work we have confirmed that Ar and N_2 can be used as actinometers, while He has a too high excitation threshold energy, and therefore cannot be used as an actinometer in our case.

We have then systematically evaluated the effect of different plasma parameters (power, pressure, flow rate) on the concentration of atomic oxygen in the oxygen plasma. The results show that the value of $[O]_r$, which is respectively determined by the ratios of O emission lines at 777.1nm and 844.6nm to Ar line at 750.4nm, would be raised as the results of increasing the applied power (or power density) and pressure. We have also evaluated $[O]_r$ as a function of position within the plasma zone: it has been found that non-uniform distribution of applied MW and RF fields leads to the corresponding $[O]_r$ distribution in the three excitation modes.

We have demonstrated the two different O emission lines (777.1nm and 844.6nm) can be successfully used as the measure of $[O]_r$. This has been correlated with other published data.

In the last part of this work we investigated $[H]_r$ in the methane plasma. We have demonstrated the beneficial role of adding Ar or N_2 to CH_4 to enhance dissociation of CH_4 , leading to a higher amount of $[H]_r$. This correlated well with the previous work from this laboratory on the growth of a C:H films in MW/RF plasma.

By successfully measuring $[O]_r$ and $[H]_r$, our work shows that the actinometry is a useful method to monitor the relative concentration of species under consideration in the plasma diagnostic techniques.

REFERENCES

1. J.R. HOLLAHAN and A.T. BELL, Techniques and Applications of Plasma Chemistry, (John Wiley & Sons, Inc., 1974)

2. L. MARTINU, A. RAVEH, A. DOMINGUE, L. BERTRAND, J.E. KLEMBERG-SAPIEHA, S.C. GUJRATHI and M.R. WERTHEIMER, "Hard carbon film deposited under high ion flux", Thin Solid Films, **208**, 42(1992)

3. J.E. KLEMBERG-SAPIEHA, O.M. KUTTEL, L. MARTINU, and M.R. WERTHEIMER, "Dual-frequency N_2 and NH_3 plasma modification of polyethylene and polyimide", J. Vac. Sci. Technol. **A9**, 2975(1991)

4. L. MARTINU and M.R. WERTHEIMER, "Ion assisted low plasma processing: status, future, and the dual microwave-radio frequency approach", 9th Symp. Elementary Processes and Chem. Reactions in Low Temp. Plasma, Casta (Czechoslovakia), Sept.7-11, 1992

5. J.R. PARASZCZAK, J.E. HEIDENREICH, M. HATZAKIS, and M. MOISAN, "Methods of creation and effect of microwave plasmas upon the etching of polymers and silicon", Microelectronic Eng. **3**, 397(1985)

6. L. MARTINU, J.E. KLEMBERG-SAPIEHA, and M.R. WERTHEIMER, "Dual-mode microwave/radio frequency plasma deposition of dielectric thin films", Appl. Phys. Lett. **54**, 2645(1989)

7. A. RAVEH, J.E. KLEMBERG-SAPIEHA, L. MARTINU, and M.R. WERTHEIMER, "Deposition and properties of diamond-like carbon film produced in microwave and radio-frequency plasma", J. Vac. Sci. Technol. **A10**, 1723(1992)

8. J.E. KLEMBERG-SAPIEHA, O.M. KUTTEL, L. MARTINU, and M.R. WERTHEIMER, "Dual microwave-rf plasma deposition of functional coatings", Thin Solid Films, **193**, 1194(1990)

9. M. MOISAN, C. BARBEAU, R. CLAUDE, C.M. FERREIRA, J. MARGOT, J. PARASZCZAK, A.B. SA, G. SAUVE, and M.R. WERTHEIMER, "Radio frequency or microwave plasma reactors? factors determining the optimum frequency of operation", J. Vac. Sci. Technol. **B9**, 8(1991)

10. M.R. WERTHEIMER and M. MOISAN, "Comparison of microwave and lower frequency plasmas for thin film deposition and etching", J. Vac. Sci. Technol. **A3**, 2643(1985)

11. Y. TOBINAGA, N. HAYASHI, H. ARAKI, and S. NAKAYAMA, "Anisotropy of low-energy ion etching via electron cyclotron resonance", J. Vac. Sci. Technol. **B6**, 272 (1988)

12. O. JOUBERT, J. PELLETIER, and Y. ARNAL, "The etching of polymers in oxygen-based plasmas: a parametric study", J. Appl. Phys. **65**, 5096(1989)

13. M.A. HARTNEY, D.W. HESS, and D.S. SOANE, "Critical review: oxygen plasma etching for resist stripping and multilayer lithography", J. Vac. Sci. Technol. **B7**, 1(1989)

14. S.W. PANG, K.T. SUNG, and K.K. KO, "Etching of photoresist using oxygen plasma generated by a multipolar electron cyclotron resonance source", J. Vac. Sci. Technol. **B10**, 1118(1992)

15. O. JOUBERT, J. PELLETIER, C. FIORI, and T.A. TAN, "Surface mechanisms in O_2 and SF_6 microwave plasma etching of polymers", J. Appl. Phys. **67**, 4291(1990)

16. L. LEGER, J. VISENTINE, and B. SANTS-MASON, "Selected materials issues associated with space station", Proc. 18th International SAMPE Technical Conf., Oct.1986

17. W.D. MORISON, R.C. TENNYSON, J.B. FRENCH, T. BRAITHWAITE, M. MOISAN and J. HUBERT, "Atomic oxygen studies on polymers", Proc.15th Space Simulation Conf., Williamsburg, VA., Oct. 1988, NASA Conf.Publ. 3015, p.89

18. L. MARTINU, "Aging processes in diamond-like carbon and carbon/metal films", NATO ASI Ser. **B: Vol.266**, p. 467, Plenum, New York, 1991

19. O.M. KUTTEL, L. MARTINU, D. POITRAS, J.E. KLEMBERG-SAPIEHA, and M.R. WERTHEIMER, "Diamond-like carbon films deposited in dual microwave/radio frequency plasma", Mater. Sci. Eng. **B11**, 321(1992)

20. B.V. SPITSYN, L.L. BOUILOV, and B.V. DERJAGUIN, "Vapor growth of diamond on diamond and other surface", J. Cryst. Growth. **52**, 219(1981)

21. Y. SAITO, K. SATO, H. TANAKA, K. FUJITA, and S. MATUDA, "Diamond synthesis from methane-hydrogen-water mixed gas using a microwave plasma", J. Mater. Sci. **24**, 293(1989)

22. D. HUANG, M. FRANKLACH, and M. MARONCELLI, "Energetics of acetylene-addition mechanism of diamond growth", J. Phys. Chem. **92**, 6379(1988)

23. C.V. DESHPHANDEY and R.F. BUNSHAH, "Diamond and diamondlike films: deposition processes and properties", J. Vac. Sci. Technol. **A7**, 2294(1989)

24. T. MIZUTANI and S. NISHIMATSU, "Generation of low-energy neutral beams and radiation damage of SiO_2/Si by neutral bombardmant", J. Vac. Sci. Technol. **B7**, 547(1989)

25. F. PASIERB, A.GHANBARI, M.S. AMEEN, and P.S. HEINRICH, "Characterization of a novel microwave stripper", J. Vac. Sci. Technol. **A10**, 1096(1992)

26. E.M. LISTON, "Plasma treatment for improved bonding: a review", J. Adhesion, **30**, 199(1989)

27. A.M. WROBEL and G. CZEREMUSZKIN, "Effect of uv irradiation of the film during plasma chemical vapour deposition", Thin Solid Films, **216**, 203(1992)

28. R. A. GOTTSCHO, G.R. SCHELLER, and D. STONEBACK, "The effect of electrode area on low-frequency glow discharge", J. Appl. Phys. **66**, 492(1989)

29. R.W. DREYFUS, J.M. JASINSKI, R.E. WALKUP, and G.S. SELWYN, "Optical diagnostics of low pressure plasma", Pure and Appl. Chem. **57**, 1265(1985)

30. R. DEUTSCH and E. RAUCHLE, "Hysteresis effects in the plasma-electrode boundary sheath for frequencies of the order of the ion plasma frequency", Plasma Chem. Plasma Procss. **11**, 501(1991)

31. R. D'AGOSTINO, F. CRAMAROSSA, SANTOLO DE BENEDICTIS, and F. FRACASSI, "Optical emission spectroscopy and actinometry in CCl_4-Cl_2 radiofrequency discharges", Plasma Chem. Plasma Process. **4**, 163(1984)

32. J.W. COBURN and M. CHEN, "Optical emission spectroscopy of reactive plasmas: a method for correlating emission intensities to reactive particle density", J. Appl. Phys. **51**, 3134(1980)

33. J.W. COBURN and M. CHEN, "Dependence of F atom density on pressure and flow rate in CF_4 glow discharges as determined by emission spectroscopy", J. Vac. Sci. Technol. **18**, 353(1981)

34. V.M. DONNELLY, D.L. FLAMM, W.C. DAUTREMONT-SMITH, and D.J. WERDER, "Anisotropic etching of SiO_2 in low-frequency CF_4/O_2 and NF_3/Ar plasmas", J. Appl. Phys. **55**, 242(1984)

35. D.E. IBBOTSON, D. L. FLAMM, and V.M. DONNELLY, "Crystallographic etching of GaAs with bromine and chlorine plasma", J. Appl. Phys. **54**, 5974(1983)

36. H.-J. TILLER, D.BERG. and R. MOHR, "Decomposition of CCl_4 in an RF discharge-a gas chromatography and time-resolved emission spectroscopy study", Plasma Chem. Plasma Process. **1**, 247(1985)

37. R.E. WALKUP, K.L. SAENGER, and G.S. SELWYN, "Studies of atomic oxygen in O_2+CF_4 RF discharges by two-photon laser-induced fluorescence and optical emission spectroscopy", J. Chem. Phys. **84**, 2688(1986)

38. J. AMORIM, J. NAHORNY, D. PAGNON, M. TOUZEAU, M. VIALLE, R. CABANEL, and A. SCHUHL. "Monitoring an oxygen atomic source by actinometry", ISPC-10. Bochum, Aug.(1991). 2.1-30 p.1

39. J.A. MUCHA, D.L. FLAMM, and D.E. IBBOTSON, "On the role of oxygen and

hydrogen in diamond-forming discharge", J. Appl. Phys. **65**, 3448(1989)

40. L. St-ONGE, M.SC. Thesis, "Caractérisation de décharges d'hydrogéne entretenues par un champ de haue fréquence (40-2450MHz) et optimisation de leur rendement en hydrogéne atomique", Departmet of Physics, University of Montreal, 1992

41. Y. MURARKA, H. YAMASHITA, K. SATO, and H. MIYADERA, "The role of hydrogen in diamond synthesis using a microwave plasma in a CO/H_2 system", J. Appl. Phys. **67**, 6247(1990)

42. P.W. PASTEL and W.J. VARHUE, "The effect of radio frequency substrate biasing in the deposition of diamond-like carbon films in an electron cyclotron resonance discharge", J. Vac. Sci. Technol. **A9**, 1129(1991)

43. W.R.S. GARTON, Spectroscopy in the vacuum ultraviolet, in Advances in atomic and molecular physics, eds. D.R. BATES AND I. ESTERMANN, (Academic, New York, 1966)

44. REZA SAFARI, Thesis D.Sc.A., "Décharges micro-ondes en écoulement dans les mélanges oxygène-azote comme sources d'oxygène atomic et singulet, comparaison à d'autres type de plasmas", Universite PARIS-SUD (1992)

45. J.P. BOOTH, O. JOUBERT, and J. PELLETIER, "Oxygen atom actinometry reinvestigated: comparison with absolute measurements by resonance absorption at 130nm", J. Appl. Phys. **69**, 618(1991)

46. L. VRIENS, "Energy balance in low-pressure gas discharges", J. Appl. Phys. **44**, 3980 (1973)

47. S.M. ROSSNAGEL and H.R. KAUFMAN, "Langmuir probe characterization of magnetron operation", J. Vac. Sci. Technol. **A4**, 1822(1986)

48. T.E. SHERIDAN, M.J. GOECKNER, And J. GOREE, "Obervation of two-temperature electrons in a sputtering magnetron plasma", J. Vac. Sci. Technol. **A9**, 688(1991)

49. W. L. WIESE, M. W. SMITH, and B. W. GLENNON: Atomic Transition Probabilities II, National Bureau of Standards Publication, N_o.NSRDS-BS22, 1969

50. R.G. BOSISIO, C.F. WEISSFLOCH, and M.R. WERTHEIMER, "The large volume microwave plasma generator (LMP™): a new tool for research and industrial processing", J. Microwave Power **7**, 325(1972)

51. A.M. MEARNS and A.J. MORRIS, "Production of oxygen atoms in quartz and polytetrafluoroethylene discharge tubes", Nature **225**, 59(1970)

52. J. PARASCZAK, J. HEIDENREICH, "Semicoductor processing applications of microwave plasmas", NATO ASI Ser. **B: Vol.302**, p.445, Plenum, New York,1991

53. G. OELERICH-HILL, I. PUKROPSKI, and M. KUJAWKA, "On the characterization of a RF parallel plate discharge", J. Phys. D: Appl. Phys. **24**, 593(1991)

54. M. HAVERLAG, G.M.W. KROESEN, T.H.J. BISSCHOPS, andF.J. De HOOG, "Measurement of electron densities by a microwave cavity method in 13.56-MHz RF plasmas of Ar, CF_4, CF_6, and CHF_3", Plasma Chem. Plamsa Process. **11**, 357(1991)

55. F. KAUFMAN, "The air afterglow and its use in the study of some reactions of atomic oxygen", Proc. Roy. Soc. (London) **A246**, 123(1958)

56. P.D. FRANCIS, "The production of oxygen atoms in a microwave discharge and the recombination kinetics in a gas flow system", J. Phys. D: Appl. Phys. **2**, 1717(1969)

57. R.N. RUDOLPH and J.H. MOORE, "Plasma polymerization and a-C:H film ablation in microwave discharge in methane diluted with argon and hydrogen", Plasma Chem. plasma Process.**10**, 451(1990)

58. D.E. TEVAULT, "Plasma reactions of methane in nitrogen and nitrogen/oxygen carriers by matrix isolation FTIR spectroscopy", Plasma Chem. Plasma Process. **5**, 369(1985)

APPENDIX

APPENDIX I

VACUUM ULTRAVIOLET SPECROSCOPY

As mentioned in section 1.1, low pressure plasma can be used for modification of polymeric surfaces. During such treatment, three different effects can contribute to the modified surface chemical and physical properties; namely (i) chemical reaction with active species, (ii) ion-bombardment, and (iii) radiation in the UV and VUV regions.

These three effects act simultaneously, and their individual contribution to the surface properties is not yet well understood.

The role of UV and VUV radiation can be studied using optical filters to allow only a portion of the spectral range above the cut-off wavelength to illuminate the polymeric surface (Refs. I.1 and I.2). Such a study has been performed in this laboratory using N_2 and NH_3 plasmas (Ref. I.3). In the following, the spectra in the UV and VUV regions are shown for gases which are used for surface modification and coating of polymers. This experiments involve the analysis of the VUV radiation from O_2, CH_4, Ar, H_2, and N_2 in MW, RF and MW/RF discharges. In all experiments the gas pressure is 0.1Torr and the total flow rate is 55sccm; the RF and MW power is 150W, and the combination of 150W RF and 150W MW power is used for the MW/RF discharge.

In the following cases, the identification of wavelengths (see Table A.I.1) are made mainly from the published works of Pearse and Gaydon (Ref. I.4) and Samson (Ref. I.5).

Figure A.1.1 shows the UV and VUV spectra in the oxygen plasmas. In oxygen, the radiation is mainly due to the atomic line at 130.5nm. The weak line from oxygen at 115.2nm can be observed. The impurity line from hydrogen at 121.5nm (Lyman α line),

and the line from OH at 308.9nm can also be observed. The few number of lines from about 158.0nm to 182.0nm can not be identified so far. The most intense spectrum is obtained in the MW/RF discharge. However, the peaks are weaker in MW than in RF plasma. Notice that the amplitude scale is logarithmic; the peak value ratio of the O 130.5nm resonance line are $I_{MW/RF}/I_{MW} = 4.4$ and $I_{RF}/I_{MW} = 2.9$.

Figure A.1.2 shows the UV and VUV spectra from methane plasmas, where we again observe that MW/RF plasma yields the most intense radiation, while the radiation in RF plasma is slightly higher than that in its MW counterpart. For example, the calculation of the most intense peak value in CH_4 discharge shows that $I_{MW/RF}/I_{MW} = 4$, and $I_{RF}/I_{MW} = 1.18$. The identified lines in the CH_4 spectrum are CH_3 lines at 149.9nm and 138.6nm; the hydrogen Lyman α line at 121.5nm. The major lines remain unidentified in CH_4 because only few identified wavelength data are available in the literature.

Figure A.1.3 shows the UV and VUV spectra in Ar discharge, where the intensities of RF emissions are again seen to be larger than that of their MW counterpart. However, the MW/RF emissions are somewhat weaker than RF emisson in this case. The experimental data show that the RF bias in MW/RF discharge is by about 100V lower than that in RF discharge at same RF power level. This fact suggests that the RF bias affects strongly the emission intensity. In argon, the radiation is mainly due to the Ar lines, which are listed in Table A.I.1. Although the hydrogen line at 125.1nm and atomic oxygen line at 130.5nm can be observed. There are considerable number of lines, from 140.0nm to 220.0nm, which remain unidentified.

The UV and VUV spectra of H_2 and N_2 are shown in Figures A.1.4 and A.1.5, respectively. Similarly to results above, RF plasma yields more intense radiation than MW. But, there is no significant increase in intensity for the MW/RF case in comparison with RF (for N_2, there even is a decrease in region 200-250nm). The RF bias is also found to

decrease somewhat in the MW/RF case compared with pure RF at equal RF power. In hydrogen, there is a well known emission line in VUV region; the Lyman α line at 121.5nm, which is very intense in all cases in present experiment. The most intense atomic nitrogen line observed in nitrogen is 120.0nm. The major radiation is mainly due to the molecular nitrogen, and the most intense emission characteristics are listed in Table A.I.1.

In the UV and VUV radiation studies, systematic work is necessary to address the following issues: (i) identify the UV emission lines of gases used for plasma processing (ii) parametric study of UV radiation.

References

I.1. M. HUDIS, Chapter 3 of Techniques and Applications of Plasma Chemistry, ed. by J.R. Hollahan and A.T. Bell, (John Wiley & Sons, Inc., 1974)

I.2. M. HUDIS, "Surface crosslinking of polyethylene using a hydrogen glow discharge", J. Appl. Polymer Sci. **16**, 2397(1972)

I.3. J.E. KLEMBERG-SAPIEHA, O.M. KUTTEL, L. MARTINU, and M.R. WERTHEIMER, "Dual-frequency N_2 and NH_3 plasma modification of polyethylene and polyimide", J. Vac. Sci. Technol. **A9**, 2975(1991)

I.4. R.P.B. PEARSE and A.G. GAYDON, The Identification of Molecular Spectra, (Chapma & Hall LTD, 1963)

I.5. J.A.R. SAMSON, Techniques of Vacuum Ultraviolet Spectroscopy, (John Wiley & Sons, Inc., 1967)

Table A.I.1. Positions of emission features in different plasmas: O_2, CH_4, Ar, H_2, and N_2 (I.4,5).

O_2 (nm)	CH_4 (nm)	Ar (nm)	H_2 (nm)	N_2 (nm)
115.2(O)	138.6(CH_3)	104.8(Ar)	121.5(H)	120.0(N)
130.5(H)	149.9(CH_3)	106.7(Ar)		149.2(N_2)
121.5(H)	121.5(H)	307.9(Ar)		174.5(N_2)
308.9(OH)		309.3(Ar)		205.9(N_2)
		338.3(Ar)		215.3(N_2)
		403.8(Ar)		236.6(N_2)
		415.9(Ar)		247.1(N_2)
		420.1(Ar)		259.2(N_2)
		425.9(Ar)		296.2(N_2)
		121.5(H)		315.9(N_2)
		130.5(O)		337.1(N_2)
				353.6(N_2)
				357.6(N_2)
				371.0(N_2)
				375.5(N_2)
				380.4(N_2)
				399.8(N_2)
				405.9(N_2)

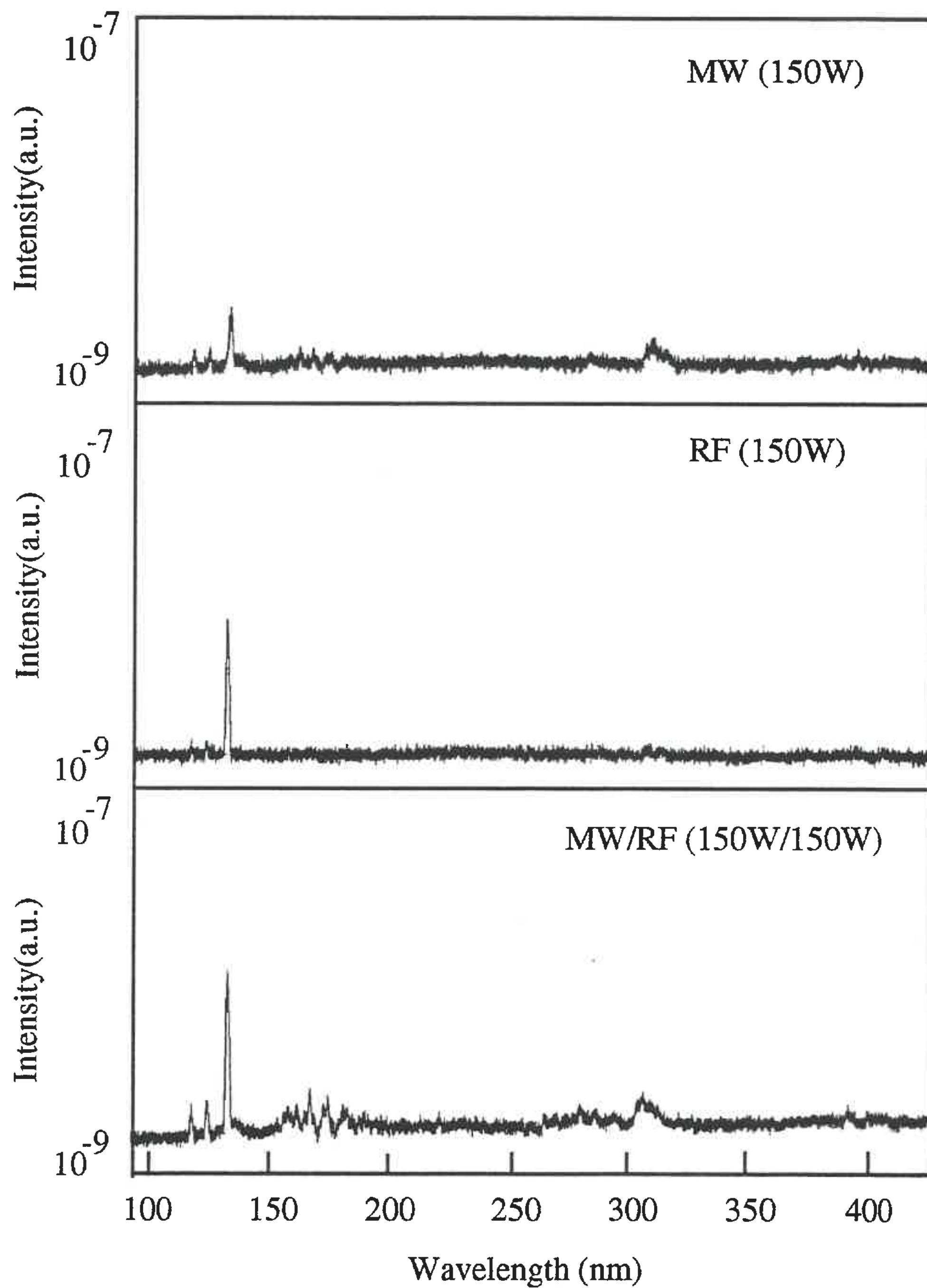

Fig.A.1.1. Oxygen UV and VUV spectra in MW, RF, and MW/RF discharges. Pressure is 0.1Torr, flow rate is 55sccm.

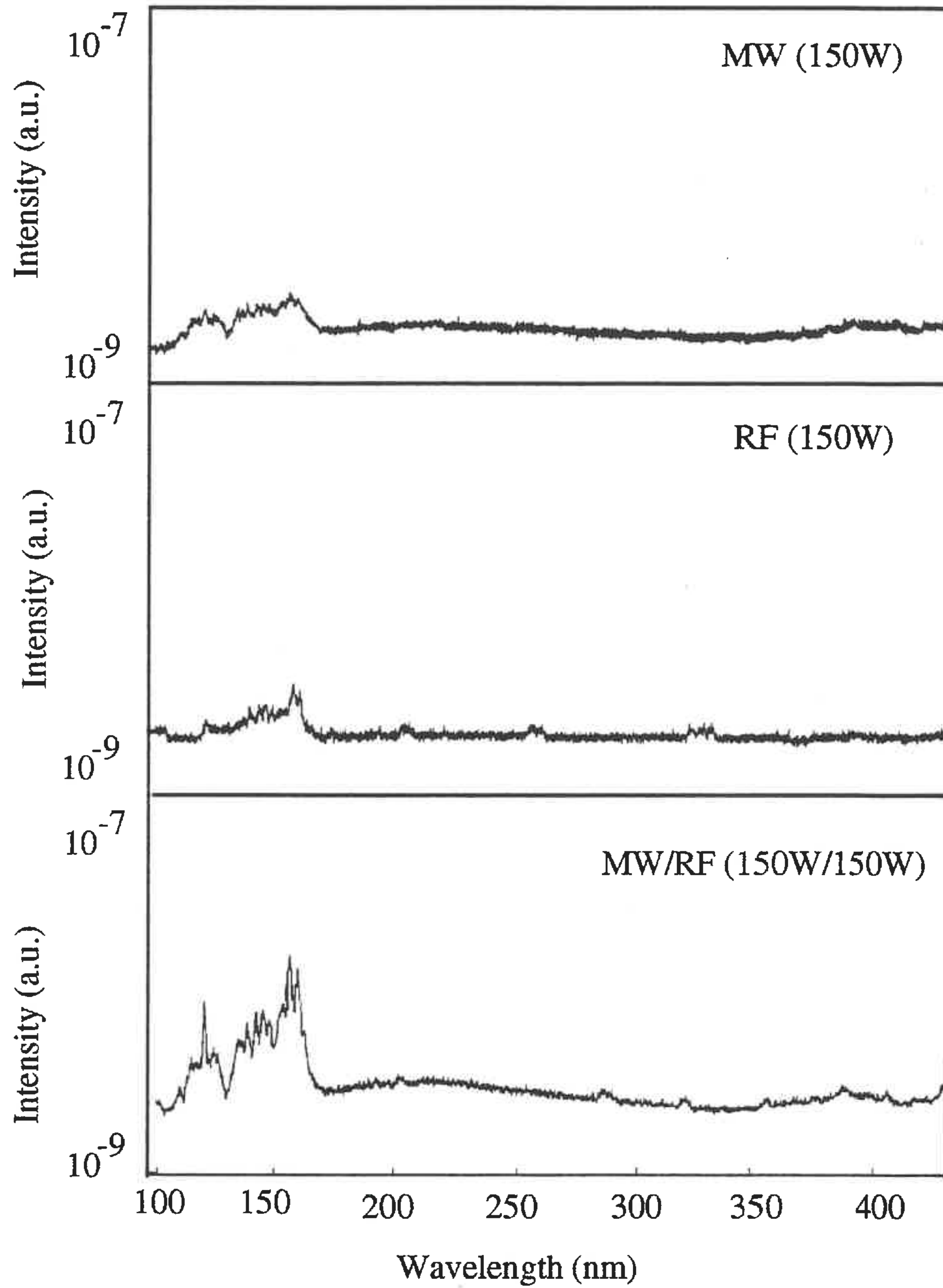

Fig.A.1.2. Methane UV and VUV spectra in MW, RF, and MW/RF discharges. Pressure is 0.1Torr, flow rate is 55sccm.

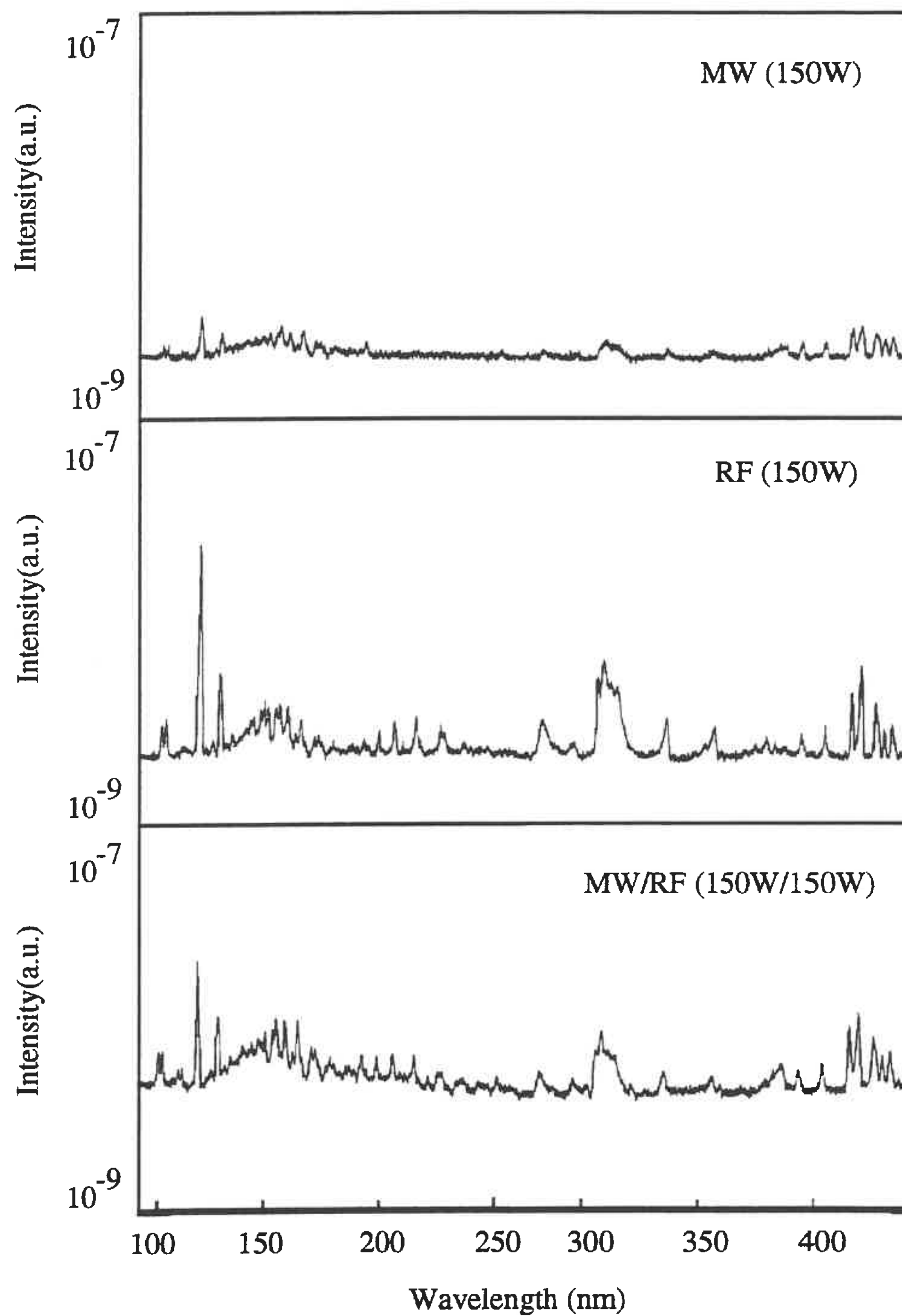

Fig.A.1.3. Argon UV and VUV spectra in MW, RF, and MW/RF discharges. Pressure is 0.1Torr, flow rate is 55sccm.

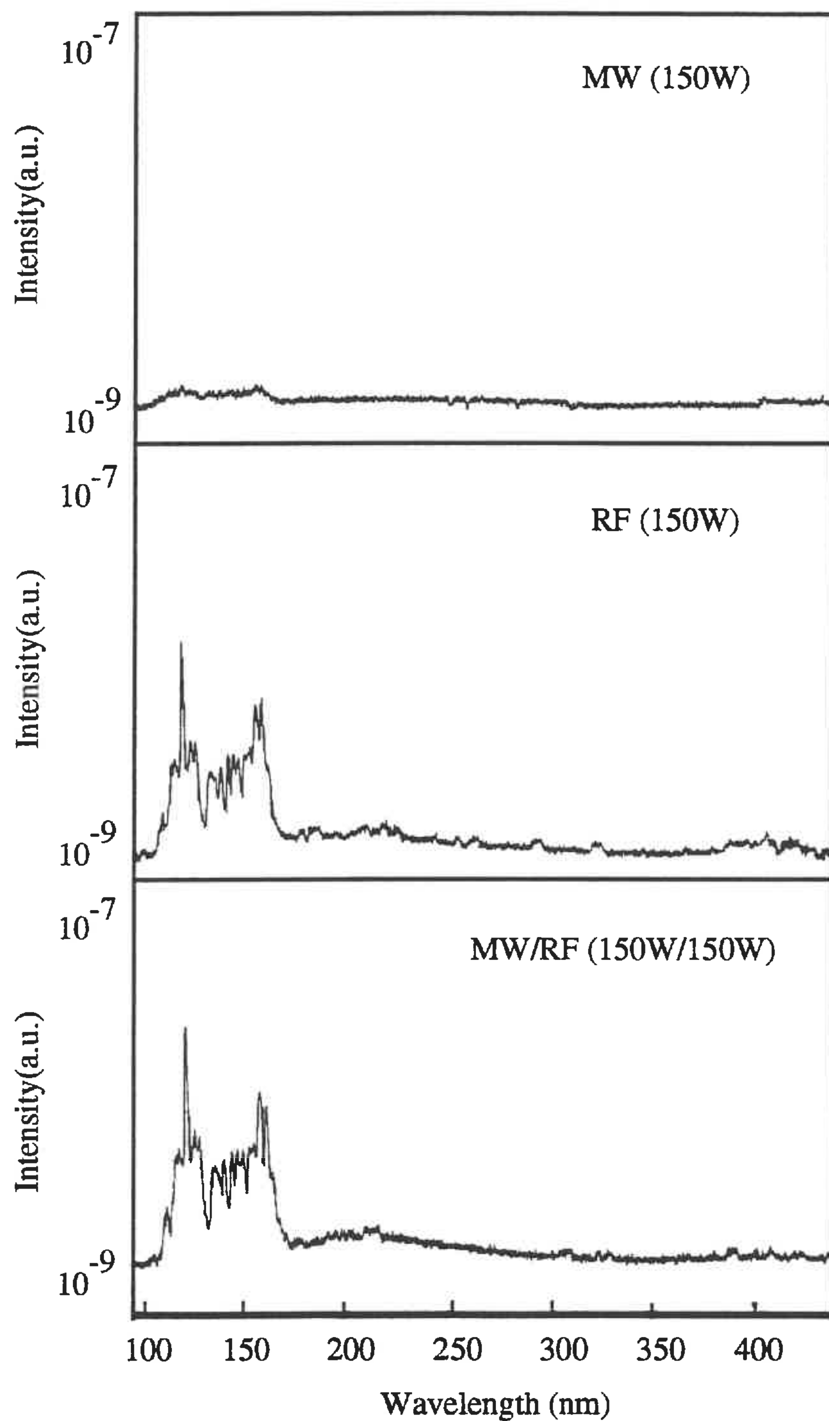

Fig.A.1.4. Hydrogen UV and VUV spectra in MW, RF, and MW/RF discharges. Pressure is 0.1Torr, flow rate is 55sccm.

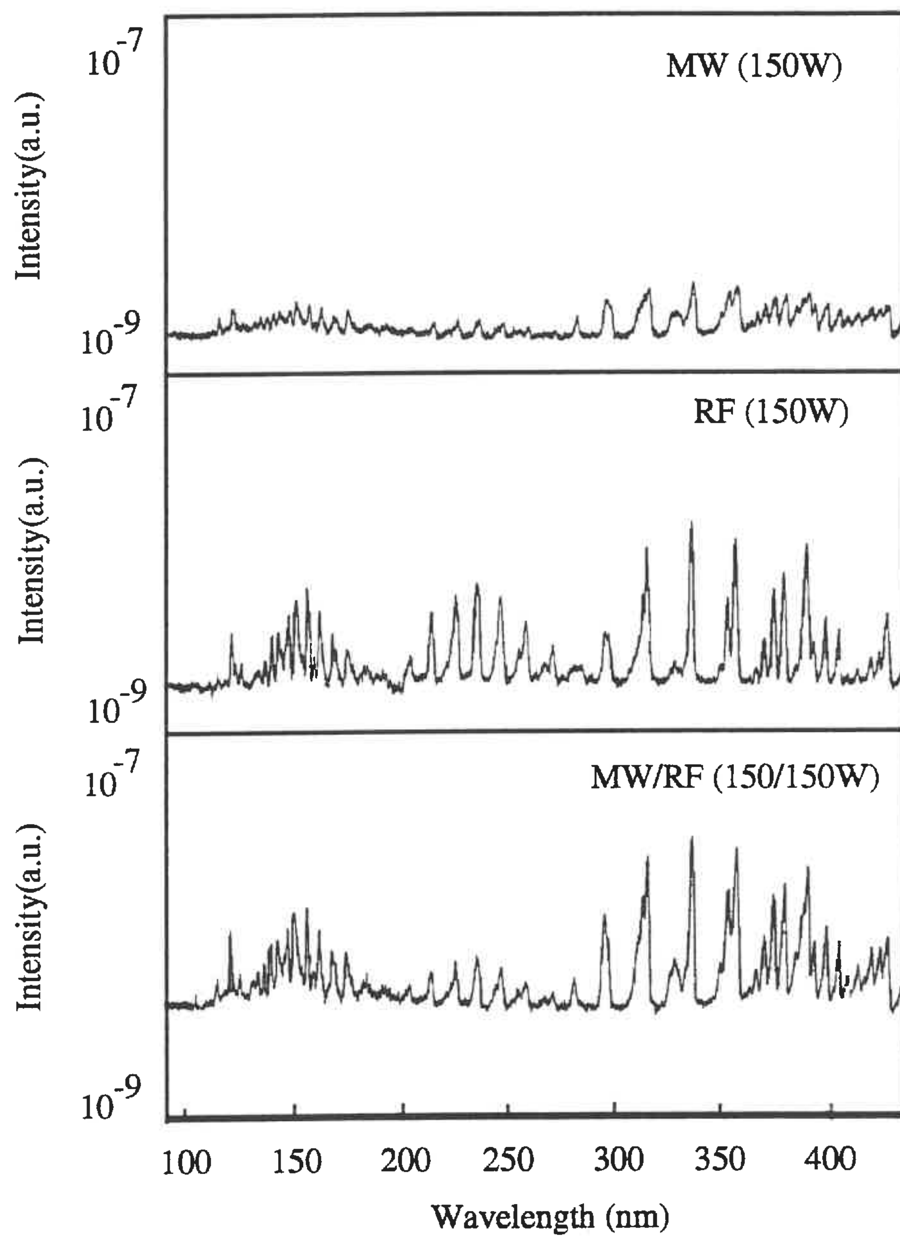

Fig.A.1.5. Nitrogen UV and VUV spectra in MW, RF, and MW/RF discharges. Pressure is 0.1Torr, flow rate is 55sccm.

APPENDIX II

MEASUREMENT OF THE TAIL ELECTRON TEMPERATURE

II.1 Model

For a low pressure discharge, the predominant excitation channel for emission is direct electron impact on ground-state species (Refs.II.1-II.3). The equation (1) is rewritten as

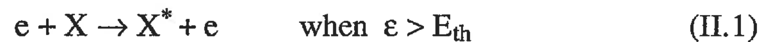

$$e + X \rightarrow X^{*} + e \qquad \text{when } \varepsilon > E_{th} \qquad \text{(II.1)}$$

Where X* indicates an excited electronic state of species X. The de-excitation of these species is postulated to occur radiatively, i.e.

$$X^{*} \rightarrow X + h\nu \qquad \text{(II.2)}$$

At steady state, the measured emission intensity I_x of a particular spectral line at transition frequency ν_x arising from excited state species X* is given by (Ref.II.4):

$$I_x = N\, h\, \nu_x\, n_e \frac{A_x}{\sum A_x} < \sigma V >_x \qquad \text{(II.3)}$$

where N is neutral atom density, n_e is electron density, A_x is transition probability, ν_x is transition frequency. The term $\langle \sigma V \rangle_x$ is given by

$$\langle \sigma V \rangle_x = \int_{E_{thx}}^{\infty} f(\varepsilon)\sigma_x(\varepsilon)\sqrt{\frac{2\varepsilon}{m_e}}\,d\varepsilon \tag{II.4}$$

From equations (II.3) and (II.4), we can obtain the optical emission intensity ratio for two lines arising from the transitions i->j and i->l of the same atomic system

$$\frac{I_{jix}}{I_{lix}} = \frac{v_{jix} A_{jix} \sum_{m<l} A_{lmx} \int_{E_{thix}}^{\infty} f(\varepsilon)\,\sigma_{ix}(\varepsilon)\sqrt{\frac{2\varepsilon}{m_e}}\,d\varepsilon}{v_{lix} A_{lix} \sum_{m<j} A_{jmx} \int_{E_{thjx}}^{\infty} f(\varepsilon)\,\sigma_{jx}(\varepsilon)\sqrt{\frac{2\varepsilon}{m_e}}\,d\varepsilon} \tag{II.5}$$

For a particular emission line, the transition frequency $v_{x(i,j,l)}$ and the probability $A_{x(i,j,m)}$ in equation (II.5) are constant. The standard method of spectroscopically measuring electron temperature using the line intensity ratio in a plasma is to replace equation (II.5) with Allen's calculated result, in which case the line ratio becomes (Ref.II. 3):

$$\frac{I_{jix}}{I_{lix}} = \left(\frac{\varepsilon_{lx}}{\varepsilon_{jx}}\right)^{1.5} \frac{\lambda_{lix}\, f_{ljx} A_{jix} \sum_{m<l} A_{lmx}}{\lambda_{jix}\, f_{llx}\, A_{lix} \sum_{m<j} A_{jmx}} 10^{5040\,(\varepsilon_{lx}-\varepsilon_{jx})/T_e} \tag{II.6}$$

The main differences between equations (II.5) and (II.6) are: (i)the excitation cross section is considered as a function of electron energy in equation (II.5), and (ii) electrons with energies above the integral limit E_{th} contribute to the intergration in equation (II.5), so that the ratio of emission intensity given by equation (II.5) only depends on tail electron energies, i.e. the tail electron temperature. It is known that electron temperature cannot be determined from measured spectral line intensities without assuming the type of equilibrium in the discharge plasma (Ref. II.3). The complete theory of a low pressure discharge would involve the problem of solving the Boltzman equation. But a simple and frequently employed alternative is to assume that the electrons have a Maxwellian distribution. We make this assumption here, that is, we do not consider the EEDF between

MW and RF plasma to be different. Based on the assumption of Maxwellian distribution, equation (II.5) allows us to calculate the emission intensity ratio as a function of the value of the tail electron temperature $T_e^{(t)}$. Comparing this theoretical emission intensity ratio with the experimental results measured by OES, we can then obtain the relationship between $T_e^{(t)}$ and plasma parameters.

II.2 Results and Discussion

The experimental MW, RF and MW/RF discharges spectra of argon are shown in Figure A.2.1. Table A.II.1 shows the emission lines in wavelength region of 600-850nm from an argon plasma.

Figure A.2.2 shows the calculated results of optical emisssion intensity ratios, which are determined by eq.(II.5), of different argon line ratios, i.e. 800.6nm/840.8nm, 800.6nm/826.5nm and 810.3nm/840.8nm. The excitation probabilities are taken from the Ref.II.5, and excitation cross section from Refs.II.6 and II.7. This calculation result gives the relationship of emission intensity ratio and $T_e^{(t)}$. With OES, the emission intensity ratio can be measured as a function of plasma parameters, such as power, pressure, etc. Comparison of the values of measured ratio and the calculation one in Figure A.2.2, the relationship of $T_e^{(t)}$ and plasma parameters can be decided. Using this method, the $T_e^{(t)}$ as a function of MW power, RF bias, pressure, and axial position is measured as follows:

Figure A.2.3(a) shows $T_e^{(t)}$ as a function of MW power. We can find that $T_e^{(t)}$ increases as the MW power increaes. Figure A.2.3(b) shows $T_e^{(t)}$ as a function of V_B ($-V_B$ is RF-induced negative bias) in RF discharge. Similar increase is found with rising V_B values.

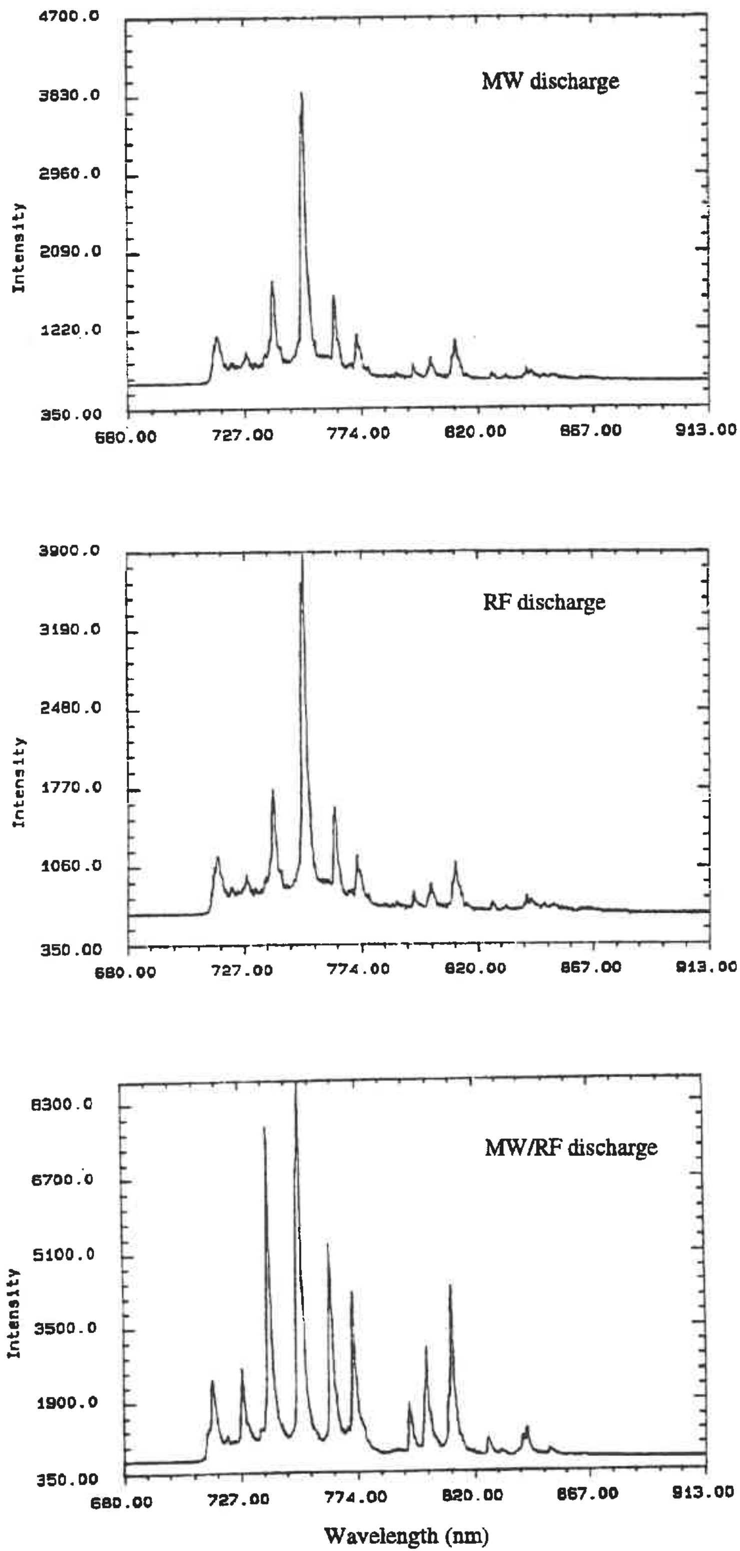

Fig.A.2.1 Optical emission spectra of Ar under MW, RF, and MW/RF conditions.

Table A.II.1 Species and transitions in an Ar glow discharge (Ref.II5)

Species	Transition	Wavelength (nm)	Threshold (eV)
Ar	4p'[3/2] - 4s [3/2]	714.7	13.279
Ar	4p'[1/2] - 4s [3/2]	727.3	13.324
Ar	4p'[3/2] - 4s [3/2]	738.4	13.298
Ar	4p'[1/2] - 4s'[1/2]	750.4	13.476
Ar	4p [3/2] - 4s [3/2]	763.5	13.168
Ar	4p [3/2] - 4s [3/2]	772.4	13.149
Ar	4p'[1/2] - 4s'[1/2]	794.8	13.279
Ar	4p [3/2] - 4s [3/2]	800.6	13.168
Ar	4p [3/2] - 4s [3/2]	810.4	13.149
Ar	4p'[1/2] - 4s'[1/2]	826.5	13.324
Ar	4p'[1/2] - 4s'[1/2]	840.8	13.298

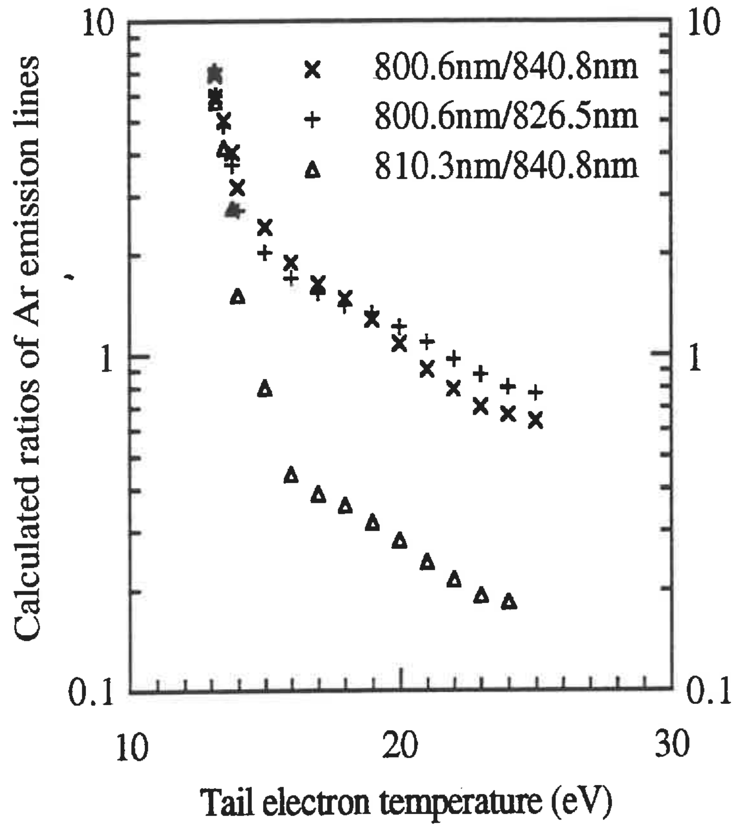

Fig.A.2.2 Calculated ratios of Ar emission intensities versus tail electron temperature based on equation (II.5).

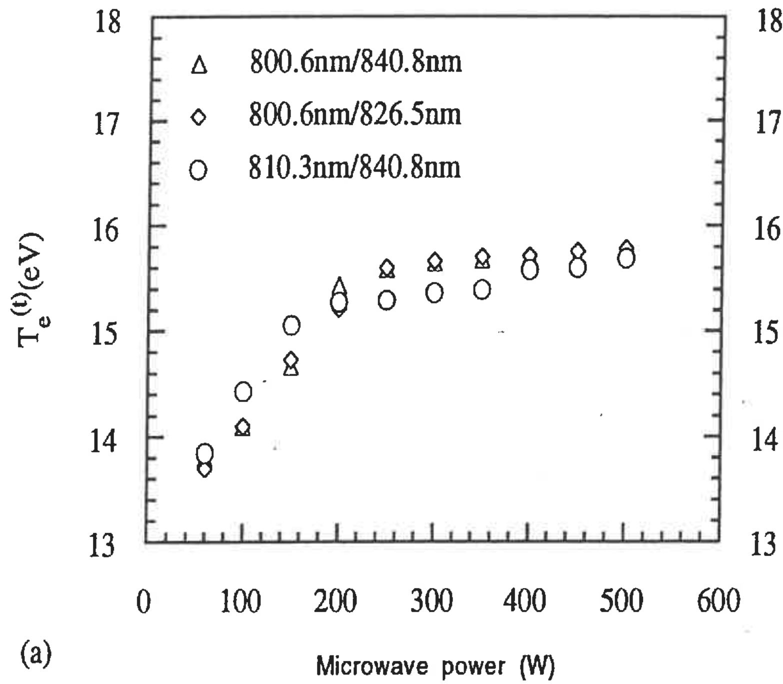

(a)

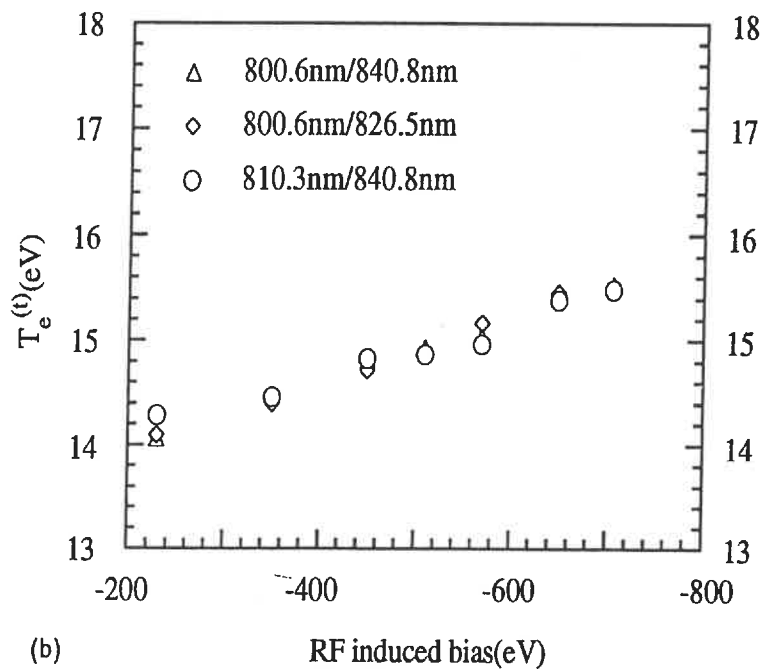

(b)

Fig.A.2.3 $T_e^{(t)}$ in Ar gas at pressure 0.1Torr and axial distance from the MW applicator d=4.8cm as a function of (a)MW power (b) RF induced bias.

The dependence of $T_e^{(t)}$ on Ar gas pressure is shown in Figure A.2.4. It can be seen that $T_e^{(t)}$ drops with the increasing pressure in both MW (Figure A.2.4(a)) and RF (Figure A.2.4(b)) plasmas.

Figure A.2.5 shows the dependence of $T_e^{(t)}$ on axial position from the MW applicator. $T_e^{(t)}$ tends lower near the RF electrode in MW plasma (see Figure A.2.5(a)). On the contrary to the MW plasma, $T_e^{(t)}$ becomes higher close to RF electrode in RF plasma (see Figure A.2.5(b)). Figure A.2.5(c) shows $T_e^{(t)}$ in MW/RF discharge, spatial profile of $T_e^{(t)}$ is different from pure MW or RF plasma, due to the different power coupling way.

Now, we discuss our results. Figure A.2.3 shows that $T_e^{(t)}$ increases with the absorb power. The increasing of excitation power would enhance the electron absorption of energy. The physical interpretation of this phenomenon is the following: as the power increases, the field strength increases. The result is that the collision frequencies of excitation and ionization become larger. Since electrons absorb energy by inelastic collisions, the increase in the collision frequency causes that the electrons gain more kinetic energy, and therefore $T_e^{(t)}$ also increases.

The relationship between the average power absorbed per electron θ (see Ref.II.8) and pressure has been calculated by Ferreira et al (Ref.II.9). For Ar discharge under RF condition, their results show that θ decreases with the increasing pressure for a given power. Recently, experimental results of Moisan et al. (Ref.II.8) verified this theoretical predictions. Moisan et al. have also shown that a similar behaviour is obtained when the excitation frequency varies from DC to 2.45GHz. In this work the decrease of $T_e^{(t)}$ in RF and MW discharges with pressure is believed to be due to a decrease in the average power absorbed per electron. Decrease of $T_e^{(t)}$ with increasing pressure was also found in RF and ECR plasmas (Refs.II.10 and II.11).

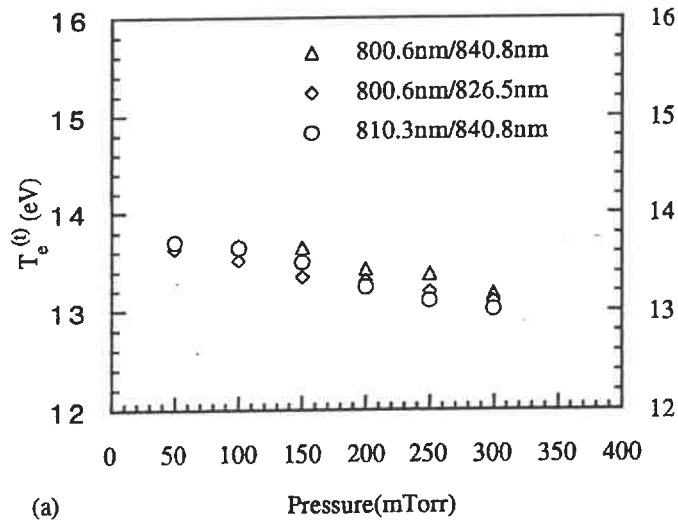

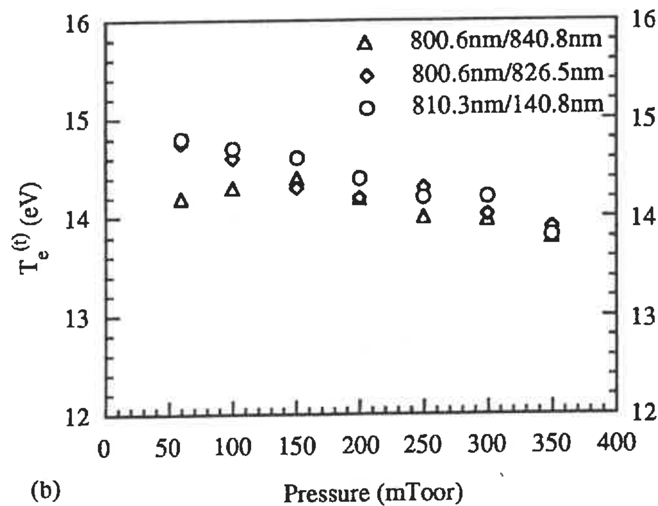

Fig.A.2.4 $T_e^{(t)}$ as a function of Ar pressure. Axial distance from MW applicator d=4.8cm. (a)MW discharge with power 60W (b)RF discharge with induced bias -570V.

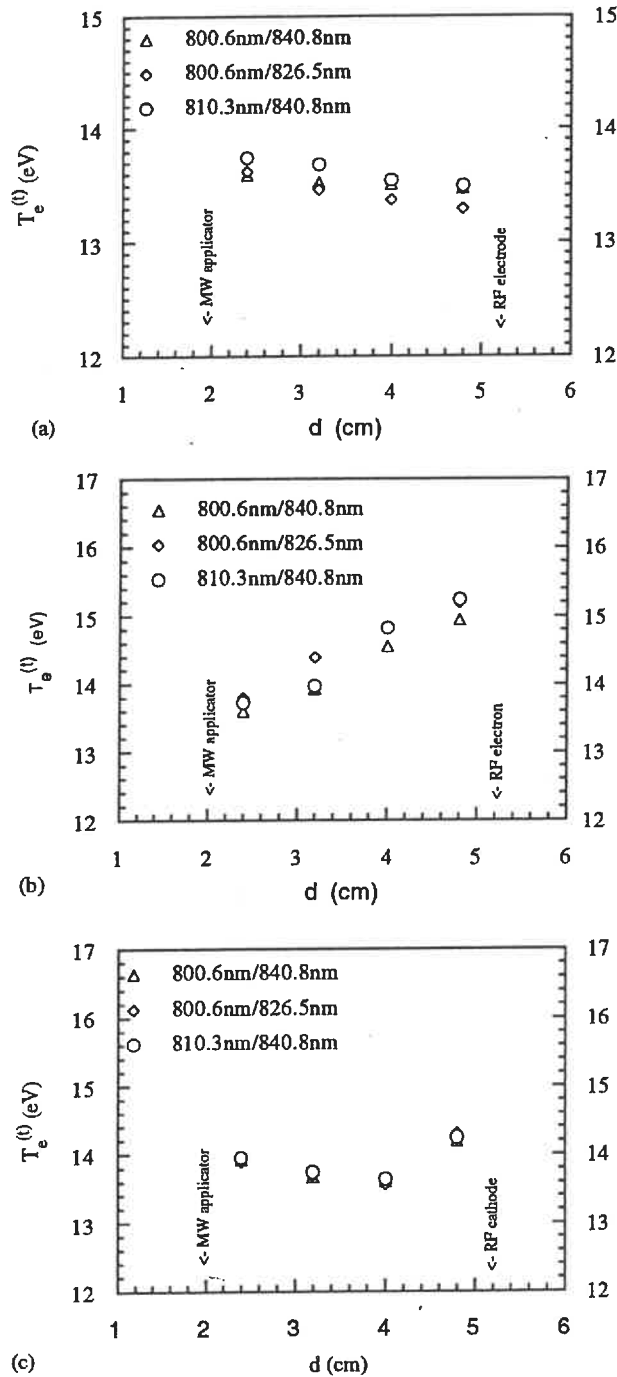

Fig.A.2.5 $T_e^{(t)}$ as a function of axial distance from the MW applicator. Ar pressure: 0.1Torr. (a)MW discharge with power: 60W (b)RF discharge with RF induced bias: -570V (c)MW/RF discharge with MW power: 60W and RF induced bias: -230V.

In the spatial dependence study, the point to be made in this experiment is that the $T_e^{(t)}$ reaches the maximum corresponding to the strong electric field location.

To study the temperature of these energetic electrons depend on further development of the energetic electron model and the measurement method. OES is one of the useful approaches in this area.

In Figures A.2.3, A.2.4, and A.2.5, the results come from different emission line ratios of argon; however, they show a similar dependence on the plasma parameters. We have reason to think that the measurement method described above is a sensitive way to study the temperature of tail electron group of 2-EGM in plasma. This can be understood by examining the excitation mechnism (see section 1.2.2). When the main excitation channel for emission is direct electron impact on ground state species, equations (II.1), (II.2), and (II.3) hold, and $T_e^{(t)}$ can be determined from the line intensity ratio given by equation (II.5). Note that the term $<\sigma V>_x$ given by equation (II.4) is significant only when electrons have energies above the excitation threshold (which is associated with the term $f(\varepsilon)\sigma_x(\varepsilon)$, and $\sigma_x(\varepsilon)$ has a value only when $\varepsilon > E_{th}$), the tail electron group is the main contribution to the excitation processes. Therefore, the information given by optical emission intensity comes from tail electrons.

This model also depends on the knowledge of EEDF. The EEDF of Ar under MW and RF conditions has been calculated by Ferreira et al. in Ref. II.9, respectively. The results show that the EEDF of MW case is different from that of RF and both of them deviate from a Maxwellian distribution. So far, there is no EEDF for MW/RF available. In the present experiment we assume that all three types of discharges (MW, RF, and MW/RF) have the Maxwellian distribution. The difference of their EEDF is not taken into account. At this stage, we can not use the numeric data of EEDF given by references

mentioned above. The main reason is that the mathematical expression of EEDF must be known in our calculation. For the further development of this method, the depedence of EEDF upon the operating parameters is suggested to be measured. And the curve fitting can be done to find the expression of EEDF, which then can be used instead of a Maxwellian distribution in equation II.5.

References

II.1. R. D'AGOSTINO, F. CRAMAROSSA, S.D.DE BENEDICTIS, and F. FRACASSI, "Optical emission spectroscopy and actinometry in CCl_4-Cl_2 radiofrequency discharges", Plasma Chem. Plasma Process. **4**, 163(1984)

II.2. R. D'AGOSTINO, F. CRAMAROSSA, V. COLAPRICO, and R. D'ETTOLE, "Mechanisms of etching and polymerization in radiofrequency discharges of CF_4-H_2, CF_4-C_2F_4, C_2F_6-H_2, C_3F_8-H_2", J. Appl. Phys. **54**, 1284(1983)

II.3. S.K.SADHYA and S.N. SEN, "Measurement of electron temperature in glow discharge in transverse magnetic field by spectroscopic method", J. Phys. D: Appl. Phys. **13**, 1275(1980)

II.4. I.M. PODGORNYI, Topics in Plasma Dignostics, (Plenum New York,1971)

II.5. W. L. WIESE, M. W. SMITH, and B. W. GLENNON: Atomic Transition Probabilities II, National Bureau of Standards Publication, N_o.NSRDS-BS22, 1969

II.6. N.T. PADIAL, G.D. MENESES, F.J. DA PAIXAO, G. CSANAK, and D.C. CARTWRIGHT, "Electron-impact excitation of the lowest four excited state of argon", Phys. Rev. **23**, 2194(1981)

II.7. J. K. BALLOU and C.C. LIN, "Electron-impact excitation of the argon atom", Phys. Rew. **8**, 1797(1973)

II.8. M. MOISAN, C. BARBEAU, R. CLAUDE, C.M. FERREIRA, J. MARGOT, J. PARASZCZAK, A.B. SA, G. SAUVE, and M.R. WERTHEIMER, "Radio frequency or microwave plasma reactors? factors determining the optimum frequency of operation", J. Vac. Sci. Technol. **B9**, 8(1991)

II.9. C.M. FERREIRA and J. LOUREIRO, "Characteristics of high-frequency and direct-current argon discharges at low pressures: a comparative analysis", J. Phys

D: Appl. Phys. **7**, 1175(1984)

II.10. J.L. JAUBERTEAU, D. DUCHESNE, C. GIRAULT, J. AUBRETON, and A. CATHEINO, "Spectroscopic study of a D.C. discharge in an argon-silane-nitrogen gas mixture under silicon nitride thin film deposition condition", Plasma Chem. Plasma Process. **10**, 589(1990)

II.11. K.L. JUNCK, M.. BRAKE, and W.D. GETTY, "Optical emission spectroscopy of electron-cyclotron-resonance-heated helium mirror plasmas", Plasma Chem. Plasma Process. **11**, 15(1991)

ÉCOLE POLYTECHNIQUE DE MONTRÉAL
3 9334 00291080 8